IEEE TRANSACTIONS ON
COMMUNICATIONS
A PUBLICATION OF THE IEEE COMMUNICATIONS SOCIETY

IEEE COMMUNICATIONS SOCIETY

MARCH 2014 VOLUME 62 NUMBER 3 IECMBT (ISSN 0090-6778)

Invited Papers and Timeliness of Review Process 769
Robert Schober, Editor-in-Chief

Backscatter Communication and RFID: Coding, Energy, and MIMO Analysis (Invited Paper) 770
Colby Boyer and Sumit Roy

COGNITIVE RADIO SYSTEMS

Antenna Selection with Power Adaptation in Interference-Constrained Cognitive Radios 786
Rimalapudi Sarvendranath and Neelesh B. Mehta

On Signal Detection in the Presence of Weakly Correlated Noise over Fading Channels 797
Farnaz Shayegh and Fabrice Labeau

Energy-Efficient Nonstationary Spectrum Sharing 810
Yuanzhang Xiao and Mihaela van der Schaar

A New Signal Structure for Active Sensing in Cognitive Radio Systems 822
Chin-Liang Wang and Han-Wei Chen

COOPERATIVE/RELAY SYSTEMS

I/Q Imbalance in AF Dual-Hop Relaying: Performance Analysis in Nakagami-*m* Fading 836
Jingya Li, Michail Matthaiou, and Tommy Svensson

Distributed Channel Coding for Underwater Acoustic Cooperative Networks 848
Amir Minayi Jalil and Ali Ghrayeb

On the Performance of Cooperative Relaying Spectrum-Sharing Systems with Collaborative Distributed Beamforming 857
Ali Afana, Vahid Asghari, Ali Ghrayeb, and Sofiene Affes

Power Adaptive Network Coding for a Non-Orthogonal Multiple-Access Relay Channel 872
Sha Wei, Jun Li, Wen Chen, Hang Su, Zihuai Lin, and Branka Vucetic

Selective Relay-Activation for Conditional DF Relaying 888
S.H. Song, Q.T. Zhang, and K. B. Letaief

Simultaneous Information and Energy Transfer in Large-Scale Networks with/without Relaying 900
Ioannis Krikidis

MIMO

Amplifier-Aware Multiple-Input Single-Output Capacity 913
Daniel Persson, Thomas Eriksson, and Erik G. Larsson

Capacity Bounds for MIMO Microwave Backhaul Links Affected by Phase Noise 920
Giuseppe Durisi, Alberto Tarable, Christian Camarda, Rahul Devassy, and Guido Montorsi

A Practical Analysis of Performance Optimization in OSTBC Based Nonlinear MIMO-OFDM Systems 930
Lei Yiming, Mairtin O'Droma, and Jin Ye

Multi-Branch Tomlinson-Harashima Precoding Design for MU-MIMO Systems: Theory and Algorithms 939
Keke Zu, Rodrigo C. de Lamare, and Martin Haardt

(Table of Contents continued on back cover)

IEEE

TransCore LP
Exhibit 1013

IEEE COMMUNICATIONS SOCIETY

The field of interest of the Communications Society consists of all telecommunications including telephone, telegraphy, facsimile, and point-to-point television by electromagnetic propagation including radio; wire; aerial; underground, coaxial, and submarine cables; waveguides, communication satellites, and lasers; in marine, aeronautical, space and fixed station services; repeaters, radio relaying, signal storage, and regeneration; telecommunication error detection and correction; multiplexing and carrier techniques; communication switching systems; data communications; and communication theory.

In addition to the above, this TRANSACTIONS contains papers pertaining to analog and digital signal processing and modulation, audio and video encoding techniques, the theory and design of transmitters, receivers, and repeaters for communications via optical and sonic media, the design and analysis of computer communication systems, and the development of communication software. Contributions of theory enhancing the understanding of communication systems and techniques are included, as are discussions of the social implications of the development of communication technology. All members of the IEEE are eligible for membership in the Society upon payment of the annual society membership fee of $25.00. Members may receive this TRANSACTIONS upon payment of an additional $42.00 (electronic) or $99.00 (print). Society members can subscribe to a Digital Library of Multiple Communications Society publications, including this one, for $134.00 (three years of access) or $249.00 (access from 1953). Please contact www.comsoc.org, www.ieee.org, or write to IEEE at the address below. *Member copies of Transactions/Journals are for personal use only.*

TRANSACTIONS EDITORIAL BOARD

L. CIMINI, *Director of Journals*
University of Delaware
Newark, MD

R. SCHOBER, *Editor-in-Chief*
University of British Columbia
Vancouver, Canada

DERRICK WING KWAN NG,
Administrative Assistant to the EIC

J. MILIZZO, *Assistant Publisher*
IEEE Communications Society
New York, NY

SENIOR EDITORS

E. AYANOGLU
University of California
Irvine, CA

D. TAYLOR
University of Canterbury
Christchurch, New Zealand

A. Zanella
IEIIT-BO/CNR
Bologna, Italy

M. Zorzi
University of Padova
Padova, Italy

EDITORS

MODULATION AND SIGNAL DESIGN
C. ABOU-RJEILY, *UWB and Diversity Methods*
Lebanese American Univ., Lebanon
S. AFFES, *Spread Spectrum and Cooperative Communications*
INRS Univ., Montreal, Canada
OZGUR BARIS AKAN, *Molecular and Nano Communications*
Koc University, Istanbul, Turkey
H. ARSLAN, *Cognitive Radio and OFDM*
Univ. of South Florida, Tampa, FL
G. BAUCH, *Coding and Relaying*
Hamburg Univ. of Technology, Hamburg, Germany
M. R. BUEHRER, *Cognitive Radio and UWB*
Virginia Tech Univ., Blacksburg, VA
C. DA SILVA, *Estimation, Detection, and Classification*
Samsung MSL, San Diego, CA
S. GEZICI, *Ultra-wideband and Detection Theory*
Bilkent Univ., Ankara, Turkey
M. JUNTTI, *MIMO and Multiple-Access*
Univ. of Oulu, Oulu, Finland
M. MATTHAIOU, *MIMO Systems and Performance Analysis*
Queen's Univ., Belfast, Northern Ireland, United Kingdom
E. PERRINS, *Area Editor*
Univ. of Kansas, Lawrence, KS
T. Q. S. QUEK, *Heterogeneous Networks and Green Communications*
Singapore Univ. of Technol. and Design (SUTD), Singapore
L. SZCZECINSKI, *Coded Modulation and ARQ*
INRS-EMT, Montreal Canada
M. VALENTI, *Adaptive Modulation and Coding*
West Virginia Univ., Morgantown, WV

WIRELESS COMMUNICATIONS
N. AL-DHAHIR, *Area Editor*
Univ. of Texas, Dallas, TX
Y. CHEN, *Performance Analysis and Cognitive Radio*
Univ. of Warwick, Coventry, United Kingdom
B. CLERCKX, *MIMO and Multipoint Techniques*
Imperial College, London, United Kingdom
H. DAI, *Cognitive Radio and Wireless Networks*
NC State Univ., Raleigh, NC
M. DI RENZO, *Heterogeneous Networks Modeling and Analysis*
CNRS – SUPELEC – Univ. Paris-Sud XI, Paris, France
A. GHRAYEB, *MIMO/Cooperative Communication*
Concordia Univ., Montreal, Canada
D. KIM, *Spread Spectrum Transmission and Access*
Sungkyunkwan Univ., Suwon, Korea
E. G. LARSSON, *Massive MIMO and Commun. Systems Optimization*
Linköping Univ., Linköping, Sweden
H. LI, *Cross-layer Design and Cyber-physical Systems*
Univ. of Tennessee, Knoxville, TN
N. B. MEHTA, *Energy Harvesting and Opportunistic Communications*
Indian Institute of Science (IISc), Bangalore, India
A. NALLANATHAN, *Smart Grid Commun. and Cognitive/Relay Networks*
King's College, London, United Kingdom
O. OYMAN, *Cooperative and Heterogeneous Networks*
Intel Corp., Santa Clara, CA
A. TAJER, *Estimation/Detection Theory and Applications*
Wayne State Univ., Detroit, MI
M. TAO, *Cooperative Communications and Resource Allocation*
Shanghai Jiao Tong Univ., Shanghai, China

T. A. TSIFTSIS, *Performance Analysis for Wireless Systems*
Technological Educational Institute of Lamia, Lamia, Greece
M. UYSAL, *Cooperative Communication and Diversity Techniques*
Ozyegin Univ., Istanbul, Turkey
J. YUAN, *PHY Layer Security and Network Coding*
Univ. of New South Wales, Sydney, Australia
A. Y. ZHANG, *Optimization and Resource Allocation*
The Chinese University of Hong Kong, Hong Kong, China

OPTICAL COMMUNICATION
J. ARMSTRONG, *Optical OFDM, MIMO, and Localization*
Monash Univ., Clayton, Australia
E. AGRELL, *Optical Modulation and Information Theory*
Chalmers Univ. of Tech., Goteborg, Sweden
C. ASSI, *Optical Network Design and Optimization*
Concordia Univ., Quebec, Canada
A. BONONI, *Area Editor*
Univ. of Parma, Parma, Italy
H. HAAS, *Optical Wireless Systems*
The Univ. of Edinburgh, Edinburgh, United Kingdom
W. C. KWONG, *Optical Networks*
Hofstra Univ., Hempstead, NY
S. HRANILOVIC, *Optical Wireless Communications*
McMaster Univ., Hamilton, Canada
S. RANDEL, *Optical MIMO and Coherent Receivers*
Bell Lab., Alcatel-Lucent, Holmdel, NJ
W. SHIEH, *Optical Transmission and Switching*
Univ. of Melbourne, Victoria, Australia
E. VARVARIGOS, *Optical Network Protocols and Performance*
Univ. of Patras, Patras, Greece

SOURCE-CHANNEL CODING AND SIGNAL PROCESSING
F. ALAJAJI, *Area Editor, Source and Source/Channel Coding*
Queen's Univ., Kingston, Canada
D. GUNDUZ, *Multi-Terminal Communications and Information Theory*
Imperial College London, London, United Kingdom
M. KIEFFER, *Coding Techniques and Multimedia Communications*
L2S, CNRS – Supelec – Univ. Paris-Sud, France
J. KLIEWER, *Iterative Methods and Cross-Layer Design*
New Jersey Institute of Technology, Newark, NJ
V. STANKOVIC, *Network Source/Channel Coding and Processing*
Univ. of Strathclyde, Glasgow, United Kingdom
M. XIAO, *Cooperative and Network Coding*
Royal Institute of Technology (KTH), Stockholm, Sweden

TRANSMISSION SYSTEMS
E. AU, *Wireless Systems*
Huawei Technologies, Ontario, Canada
G. COLAVOLPE, *Detection, Decoding, and Synchronization*
Univ. of Parma, Parma, Italy
R. DINIS, *Frequency-Domain Processing and Equalization*
Univ. Nova de Lisboa, Portugal
S. GALLI, *Wireline Systems and Smart Grid Communications*
ASSIA, Redwood City, CA
M. C. GURSOY, *QoS-Aware and Energy-Efficient Wireless Commun.*
Syracuse University, Syracuse, NY
C. LING, *Multiterminal Communications and Lattice Coding*
Imperial College London, London, United Kingdom
H. MINN, *Synchronization and Equalization*
Univ. of Texas, Dallas, TX

H. STEENDAM, *Synchronization and Multicarrier Systems*
Ghent Univ., Gent, Belgium
A. TONELLO, *Power Line Communications and Multicarrier Systems*
Univ. of Udine, Udine, Italy
G. VITETTA, *Area Editor, Equalization and Fading Channels*
Univ. of Modena, Modena, Italy
Y.-C. WU, *Sensor Networks and Synchronization*
The Univ. of Hong Kong, Hong Kong, China

NETWORKING AND CROSS-LAYER DESIGN
L. BADIA, *Network Modeling and Cross-layer Optimization*
IMT Lucca, Lucca, Italy
T. HO, *Network Information Theory and Optimization*
California Institute of Technology, CA
A. B. MACKENZIE, *Area Editor, Game Theory and Cognitive Networking*
Virginia Tech Univ., Blacksburg, VA
P. MITRAN, *Cognitive/Relay Networks and Wireless Network Coding*
Univ. of Waterloo, Waterloo, Canada
M. MOTANI, *Network Information Theory and Cooperative Protocols*
National Univ. of Singapore
P. POPOVSKI, *Wireless Network Coding and Cross-Layer Design*
Aalborg Univ., Aalborg, Denmark
W. SAAD, *Game Theory and Self-Organizing Networks*
Univ. of Miami, Miami, FL
C. W. TAN, *Optimization and Cross-Layer Design for Resource Allocation*
City Univ. of Hong Kong, Hong Kong, China
J. WIDMER, *Network Coding and Cross-Layer Design*
IMDEA Networks, Madrid, Spain
V. WONG, *Resource Management and Multiple Access*
Univ. of British Columbia, Vancouver, Canada

CODING AND COMMUNICATION THEORY
K. ABDEL-GHAFFAR, *Algebraic and LDPC Codes*
Univ. of California at Davis, CA
D. DECLERCQ, *Error Correcting Codes and Decoders*
ETIS, Cergy-Pontoise, France
L. DOLECEK, *Algabraic and Graph-based Coding Techniques*
Univ. of California, Los Angeles, CA
T. DUMAN, *Area Editor*
Arizona State Univ., Tempe, AZ
A. GRAELL I AMAT, *Concatenated Codes and Iterative Decoding*
Chalmers Univ. of Technology, Gothenburg, Sweden
A. KHISTI, *Information Theory and Physical Layer Security*
Univ. of Toronto, Toronto, Canada
M. LENTMAIER, *Codes on Graphs and Convolutional Coding*
Lunds Univ., Lund, Sweden
H. PISHRO-NIK, *LDPC Codes and Iterative Decoding*
Univ. of Massachusetts, Amherst, MA
A. RAMAMOORTHY, *Network Coding and LDPC Codes*
Iowa State Univ., Ames IA
A. THANGARAJ, *Coding Theory and Information-Theoretic Secrecy*
Indian Institute of Technology Madras (IITM), Chennai, India
T.-K. TRUONG, *Coding Theory and Techniques*
I-Shou Univ., Taiwan
P. VONTOBEL, *Coding Theory and Graphical Models*
Stanford Univ., Stanford, CA

IEEE OFFICERS

J. ROBERTO B. DE MARCA, *President and CEO*
HOWARD E. MICHEL, *President-Elect*
MARKO DELIMAR, *Secretary*
JOHN T. BARR, *Treasurer*
PETER W. STAECKER, *Past President*
SAURABH SINHA, *Vice President, Educational Activities*

GIANLUCA SETTI, *Vice President, Publication Services and Products*
RALPH M. FORD, *Vice President, Member and Geographic Activities*
KAREN BARTLESON, *President, IEEE Standards Association*
JACEK M. ZURADA, *Vice President, Technical Activities*
GARY L. BLANK, *President, IEEE-USA*

HARVEY A. FREEMAN, *Director, Division III-Communications Technology*

IEEE EXECUTIVE STAFF

E. JAMES PRENDERGAST, *Executive Director & Chief Operating Officer*

BETSY DAVIS, *Human Resources*
ANTHONY DURNIAK, *Publications Activities*
JUDITH GORMAN, *Standards Activities*
CECILIA JANKOWSKI, *Member and Geographic Activities*

DOUGLAS G. GORHAM, *Educational Activities*
PATRICK MAHONEY, *Marketing*
MATTHEW LOEB, *Corporate Strategy*
THOMAS R. SIEGERT, *Business Administration*

CHRIS BRANTLEY, *IEEE-USA*
MARY WARD-CALLAN, *Technical Activities*
ALEXANDER PASIK, *Information Technology*

IEEE TRANSACTIONS ON COMMUNICATIONS (ISSN 0090-6778) is published monthly by The Institute of Electrical and Electronics Engineers, Inc. Responsibility for the contents rests upon the authors and not upon the IEEE, the Society, or its members. IEEE Corporate Office: 3 Park Avenue, 17th Floor, New York, NY 10016-5997. IEEE Operations Center: 445 Hoes Lane, P.O. Box 1331, Piscataway, NJ 08855-1331. NJ Telephone: +1 732 981 0060. Price/Publication Information: Individual copies: IEEE Members $20.00 (first copy only), nonmembers $57.00 per copy. (Note: postage and handling charge not included.) Member and nonmember subscription prices available upon request. Available in microfiche and microfilm. Copyright and Reprint Permissions: Abstracting is permitted with credit to the source. Libraries are permitted to photocopy for private use of patrons, provided the per- copy fee indicated in the code at the bottom of the first page is paid through the Copyright Clearance Center, 222 Rosewood Drive, Danvers, MA 01923. For all other copying, reprint, or republication permission, write to Copyrights and Permissions Department, IEEE Publications Administration, 445 Hoes Lane, P.O. Box 1331, Piscataway, NJ 08855-1331.

Copyright © 2014 by The Institute of Electrical and Electronics Engineers, Inc. All rights reserved.

Periodicals postage paid at New York, NY and at additional mailing offices. Postmaster: Send address changes to: IEEE TRANSACTIONS ON COMMUNICATIONS, IEEE, 445 Hoes Lane, P.O. Box 1331, Piscataway, NJ 08855-1331. GST Registration No. 125634188. Printed in U.S.

SFI Certified Sourcing
www.sfiprogram.org
SFI-00711

RECEIVED
APR 02 2014
JACK TARVER LIBRARY
MERCER UNIVERSITY

Invited Papers and Timeliness of Review Process

By Robert Schober, Editor-in-Chief

Dear Readers:

I am writing this editorial to inform you about a new initiative that we have started and about the timeliness of our review and publication process.



Robert Schober

Our journal has one of the longest histories among all communication journals. In fact, the first issue of the *Transactions of the IRE Professional Group on Communication Systems*, which after several name changes became the *IEEE Transactions on Communications* (TCOM), was published in 1953. Throughout the years TCOM has maintained a broad scope spanning several areas such as wireless communications, wired communications, and optical communications, and served as an "incubator" for other, more specialized journals in some of these areas. Over the years, TCOM has been at the forefront of many new research directions, including spread spectrum communications, turbo coding, space-time coding, cooperative diversity, and many others. In the early years of TCOM, emerging research areas were shaped and advanced through special issues. These special issues in turn also helped TCOM to reshape and refocus its scope. However, after the creation of a dedicated "special-issues journal," the *IEEE Journal on Selected Areas on Communications*, in 1983, TCOM has ceased publishing special issues. Since then, the appointment of experts in new and emerging research areas as Editors has become our primary means for reshaping and modernizing the scope of TCOM. Although this has served us very well so far as current examples of new areas such as Physical Layer Security, Energy Harvesting, Massive MIMO, Optical Wireless, Heterogeneous and Self-organizing Networks, Molecular and Nano-Communications, etc. show, it is perhaps time to enhance the current approach by installing a more proactive mechanism again.

To this end, TCOM will start publishing invited papers on emerging research topics in communications by authors who are well known experts in their respective research areas. Besides the obvious benefit that the publication of such high quality papers provides to our readers, we hope that this initiative will also help us attract additional submissions in the respective emerging research areas. The first invited paper, authored by Colby Boyer and Sumit Roy and titled "Backscatter Communication and RFID: Coding, Energy, and MIMO Analysis," appears in the current issue. While we do not have a fixed target number, we expect to publish three or four invited papers per year. I note that although the invited papers are solicited directly by the Editor-in-Chief, they of course undergo the same rigorous review process as regular submissions.

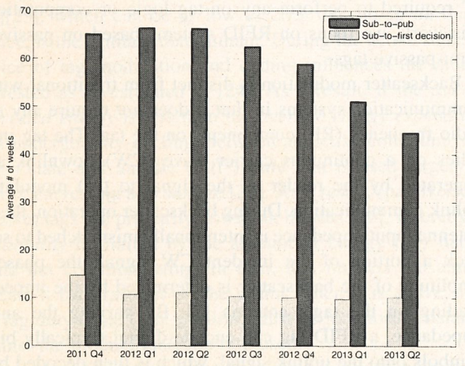


Fig. 1 Average number of weeks from submission to online posting (sub-to-pub) in IEEE Xplore [Source: IEEE Publication Services and Products] and average number of weeks from submission to first decision (sub-to-first decision) of TCOM papers. The x-axis shows the quarter (Q) in which the counted papers were published and the first decision was made, respectively.

The second issue that I would like to address is the timeliness of our review and publication process. Over the past few years, TCOM has undertaken a concerted effort to improve the timeliness of the review and publication process. The fruits of this effort, which was initiated already by my predecessor, Michele Zorzi, are shown in Fig. 1. This figure depicts the average number of weeks it takes for an accepted TCOM paper from submission to online publication in IEEE Xplore (sub-to-pub), and the average number of weeks it takes for a TCOM paper from submission to the first decision (sub-to-first decision). Over the past year, our average sub-to-pub times improved from 66.3 weeks in the second quarter of 2012 to 44.5 weeks in the second quarter of 2013. Several factors have contributed to this improvement. First, our Editors have improved the timeliness of their decisions (without compromising on quality). In fact, over the past year, the average time it takes an Editor to arrive at a first decision has stabilized at approximately 10 weeks. Second, we have decreased the time that a reviewer has to submit his/her review. Third, we decreased the time an author has to revise a paper. Fourth, we have moved the post-acceptance processing to Manuscript Central. We expect additional improvements in our timeliness over the next few quarters before we reach steady state.[1]

In summary, I believe TCOM offers a high quality and timely publication process to its authors, which will continue to attract high quality papers to the benefit of our readers. The new invited papers will further enhance the attractiveness of TCOM and help us in shaping and refining the scope of TCOM.

In closing, I would like to thank the many individuals that have contributed to the success of TCOM in the past two years. First of all, I would like to thank the Editors and Area Editors as well as the countless anonymous reviewers for the hard work and time they generously dedicated to TCOM. Their help was key in improving the timeliness of the review process without compromising on quality. Furthermore, I would like to thank the Senior Editors (Alberto Zanella, Desmond Taylor, Ender Ayanoglu, and Michele Zorzi) for sharing their wisdom with me and helping me in launching the invited papers initiative. I also would like to thank Katie Wilson (Director of Journals and VP Publications), Vincent Chan (VP Publications), and Len Cimini (Director of Journals) for their invaluable advice and support. Special thanks is due to David Daut, who served for 25 years as the Publications Editor for TCOM, and Joseph Milizzo (ComSoc Staff), who both were instrumental in moving the post-acceptance processing to Manuscript Central. Last but not least, I would like to thank the TCOM Assistant, Derrick Wing Kwan Ng, whose tireless 24/7 attitude toward all TCOM related issues has made my task as Editor-in-Chief so much easier.

[1] The sub-to-pub times for the third and fourth quarters of 2013 were not available yet at the time of publication of this editorial.

– Invited Paper –

Backscatter Communication and RFID: Coding, Energy, and MIMO Analysis

Colby Boyer, *Student Member IEEE*, and Sumit Roy, *Fellow IEEE*

***Abstract*—Radio Frequency IDentification (RFID) is intended to supplant legacy (optical) bar code scanning technology found in many logistic and retail applications. RFID is distinguished by *inexpensive, low power and compact form factor* tags, whose longevity and efficacy are predicated on using passive communication techniques and on-tag power harvesting. Such tags employ *backscatter modulation*, which does not require any active RF components. As a result, backscatter has become an attractive design choice for *short-range* communications in power constrained wireless sensor networking scenarios.**

The purpose of this work is two-fold. First, it aims to expose backscatter communication as an emerging topic to a communication systems-theoretic audience. Since backscatter modulation and on-tag power harvesting efficiency are coupled, it is necessary to re-examine notions of power and spectral efficiency from an energy-constraint perspective; this leads to novel coded modulation schemes for future RFID systems. Further, we investigate RFID MIMO systems where the channel fading encountered has different statistics than the classical Rayleigh fading model. In turn,the trade off between diversity order and spatial multiplexing gains are distinct from wide-area MIMO.

***Index Terms*—Radio communication, scattering, RFID tags, MIMO, modulation, modulation coding, fading, wireless sensor networks.**

I. Introduction

RADIO Frequency IDentification (RFID) technology is a short-range wireless communication technique for reading data such as an electronic product code (EPC) (and increasingly, other relevant information) stored on a tag affixed to objects [1]. The information on EPC-tagged objects are communicated to a nearby RFID *reader* via *backscatter modulation*, which is the focus of this work. Seen as a way to improve on the limitations of the present-day optical bar code reader systems, commercial adoption of RFID has been critically predicated on (ultra) low-cost tags. This has lead to an emphasis on *passive* tags that operate without any on-tag power source and rely entirely on backscatter, as a passive communication method, for the tag-to-reader uplink. Consequently, the maturation of passive low-cost RFID tag technology has made it a viable candidate for more general wireless sensor networking scenarios [2][3] where short-range, low rate links suffice.

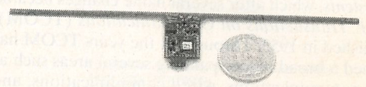


Fig. 1. The wireless identification and sensing platform (WISP) [8] is a programmable sensor platform based on RFID. It is wirelessly powered and uses backscatter modulation to relay sensor information to a RFID reader.

In general, RFID tag types may be classified into one of the following: *active*, *semi-passive*, or *passive*. Active RFID tags utilize powered transceivers for the uplink; see for reference IEEE 802.15.4f [4] regarding standardization efforts. Semi-passive tags consist of a low cost/power integrated circuit (IC) capable of limited processing, along with RF circuitry to support backscatter modulation and downlink demodulation, a rectifier to harvest RF energy, and energy storage (e.g. battery or capacitor). Passive tags can have the same general architecture as semi-passive tags, except they cannot store energy and are completely reliant on harvested RF energy. While passive *chipless* tags [5][6] are a promising area of research for reducing the cost of RFID tags, they lack the IC required to perform any on-tag logic or computation. In this work, we focus on RFID systems based on passive and semi-passive tags.

Backscatter modulation is distinct from traditional wireless communication systems in that it does *not* require any active radio frequency (RF) components on the tag. The tag instead relies on a continuous carrier wave (CW) downlink signal generated by the reader as the signal to (re) modulate for uplink communication. During backscatter operation, the tag's antenna input impedance is intentionally mismatched to scatter back a portion of the incident CW signal; the phase and amplitude of the backscatter is determined by the impedance loading on the tag's antenna [7]. By varying the antenna impedance, a RFID tag can encode digital (typically binary) symbols onto the uplink signal, which is then decoded by the RFID reader.

The ongoing integration of various sensors on RFID tags, such as described in [8] [9], confirms the potential for new sensor networks that use modified RFID components and existing protocol stacks (notably ISO 18000-6C [10], the industry standard) to transport any dynamic sensory data collected by a tag. Target applications include scenarios where traditional *active* RF systems cannot achieve required link efficiency vs. power consumption trade-offs, while meeting weight/size constraints [11]. Of particular note are low-power, constrained form-factor scenarios from biological/physiological sensing applications, for which specialized RFID tags with sensors have been fabricated [12][13][14]. An example of a RFID based sensor platform is the Wireless Integrated Sensing Platform (WISP) [8], shown in Fig. 1. As sensor systems grow in the number of users, data volume, and range, passive backscatter based networks will require improved link and power efficiencies, thereby opening a new set of challenges for RFID system designers at all (circuit, device, communication link and network stack) levels.

The existing literature on the communication theoretic aspect of backscatter focuses on improving the current uplink multiple access technique in the ISO 18000-6C standard, which uses framed slotted ALOHA [15]. Enhancements include a new space-frequency division random access scheme in [16], as well as multi-user detection [17] [18] in conjunction with rateless codes [19]. In contrast, the physical layer aspects of RFID and backscatter appear to have been largely ignored. As evidence, the ISO 18000-6C protocol does not incorporate any forward error correction or fine grained link adaptation; only simple cyclic redundancy checks are used for data integrity. The protocol's modulation scheme is based on binary line codes [20], where the only available variable to adjust the link's reliability and rate is the symbol period. Consequently the current design does not provide for a robust uplink during poor link conditions [21].

There exists considerable opportunity for communications system designers to contribute notions from coded modulation, suitably modified for RFID context, for improving uplink efficiency and/or achieving desired trade-offs. The amount of energy a tag can harvest *on average* is affected by numerous factors, depending on if the tag is idle or backscattering. During the idle state, the efficiency of the harvesting *circuitry* [22][23], which can be as low as 20% depending on design choice, is the primary determinant. During the active state, the choice of tag modulation and coding influences the amount harvested as investigated in [24]. As a result, if the *average harvested energy* is less than the *average energy expenditure*, tags undergo duty-cycling, between an active communication ('on') state and an idle ('off') state that is used largely for energy harvesting and storage [25]. As a result, (passive/semi-passive) tags are primarily downlink limited [26], whereby tag *availability* is limited by the amount of energy they harvest while not communicating. In turn, this impacts the amount of data it can transmit on the uplink when it is active, since the tag duty cycle ('on' portion) must be judiciously balanced against the modulation/code rate used.

A second distinction arises from the nature of the scattering near the tag and the reader's antennas. In backscatter, the signal received at the reader arrives after traversing two independent paths. On the reader-to-tag downlink, the impinging signal at the tag antenna is the superposition of components from multiple scatterers in the vicinity of the tag. This incident signal is modulated by the tag and scattered back to the reader; en route, the backscattered signal encounters another set of scatterers close to the reader. Since the receiver observes the product of two independent small-scale fading effects, the net fading statistics differs from the standard Rayleigh fading. Known as the dyadic backscatter channel model, first introduced and studied by [27], captures the composite fading due to the two paths and supports general multiple input multiple output (MIMO) scenarios involving M reader transmit antennas, L tag antennas, and N reader antennas. Since the dyadic channel was only recently defined, there remains ample opportunity to investigate the performance of different MIMO techniques in RFID systems.

This paper has two broad aims: to provide a tutorial survey of backscatter modulation as an emerging means for short-range low-rate communications by highlighting some relevant prior work, and to present new results on the diversity-multiplexing tradeoff of the dyadic backscatter channel. The material is organized into the following three areas:

- *Backscatter Modeling*: Section II-A provides a short tutorial review of backscatter communication *principles* [24][1], and describes the relationship between the tag equivalent circuit model and the backscattered baseband signal observed by the reader [7], [22].
- *Coding & Modulation*: Section II-B presents a summary of results from [24] on the relationship between on-tag power harvesting and forward error correction applied to higher-order backscatter constellations [28]. Using link budgets [26], [29] and a simplified tag energy harvesting model, Section II-C presents new results on the tradeoff between tag duty-cycling and link reliability for downlink limited tags.
- *MIMO*: Section III provides a tutorial review of the dyadic backscatter channel (DBC) and corresponding statistical characterization by [27]; space-time code performance results are taken from [30]. Section IV contains our primary novel contribution in this work, that derives the diversity-multiplexing tradeoff [31] for the DBC.

II. RFID Backscatter Communication Principles

A. RFID Backscatter Fundamentals

A backscatter communication system consists of two components: a RFID tag (backscatter node) and a RFID reader (transmitter/receiver) [1]. The tag does not utilize any active RF components, but the reader uses typical active RF electronics to generate a sinusoidal continuous wave (CW) signal and to demodulate the backscatter. Any tag within range of the reader's downlink CW signal will backscatter a portion back to the source (the reader), while the remainder is harvested[1] to assist powering the on-tag integrated circuit (IC). The IC modulates information onto the backscattered CW by controlling the front-end impedance loading [8], [32], as described later.

The backscattered wave observed at the reader is composed of two different components: *structural mode* and *antenna mode* scattering [7]. Structural mode scattering depends on the antenna geometry and material, but is *independent of the antenna's impedance load*. Antenna mode scattering depends

[1] via AC-to-DC conversion

Manuscript received June 6, 2013; revised October 1, 2013. The editor coordinating the review of this paper and approving it for publication was A. Zanella.

The authors are with the Department of Electrical Engineering, University of Washington, Seattle, WA 98195, USA (e-mail: {csboyer, sroy}@u.washington.edu). C. Boyer is the corresponding author.

This work was supported in part by NSF under grant ECS 0824265 and in part by MIT Lincoln Labs.

Digital Object Identifier 10.1109/TCOMM.2013.120713.130417

0090-6778/14$31.00 © 2014 IEEE

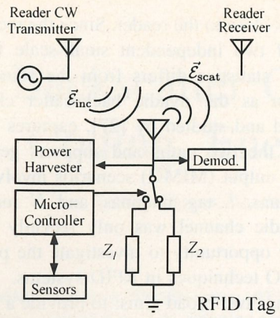


Fig. 2. System level diagram of an RFID tag with two modulator states. $\vec{\mathcal{E}}_{\text{inc}}$ represents the incident E-field generated by the reader's CW at the tags antenna. $\vec{\mathcal{E}}_{\text{scat}}$ represents the backscatter E-field propagating back to the reader's receiver. To modulate $\vec{\mathcal{E}}_{\text{scat}}$, the on-tag microcontroller logic switches the backscatter modulator between two impedance states Z_1 and Z_2. Additionally, the microcontroller processes any sensory data. The demodulator (demod.) block decodes the reader to tag communication. The power harvester captures part of the energy in the incident RF $\vec{\mathcal{E}}_{\text{inc}}$ for use by the tag.

on the antenna's load impedance. By altering the tag's antenna impedance loading, a return signal with different phase and amplitude is backscattered to the reader. The reader uses the received backscattered signal to estimate the different modulation states at the tag. A simple example of backscatter modulation is switching the tag impedance between two values, Z_1 and Z_2, to achieve binary modulation (e.g. on-off keying), as illustrated in Fig. 2. In this example, a tag is illuminated with an incident RF electrical field $\vec{\mathcal{E}}_{\text{inc}}$, part of which is backscattered as the field $\vec{\mathcal{E}}_{\text{scat}}$. The remaining power is assumed harvested by the tag, i.e. dissipated by the modulator impedances Z_1, Z_2.

To understand how the antenna's impedance load affects the backscattered and absorbed signal components, consider the Thevenin equivalent circuit of the tag front-end [7], [22]. Fig. 3 illustrates the three main system parameters V_{OC} (sinusoid voltage induced by the reader's incident CW $\vec{\mathcal{E}}_{\text{inc}}$), $Z_A = R_A + jX_A$ (antenna impedance), and $Z_L = R_L + jX_L$ is the equivalent tag impedance as shown in Fig. 3. Given the incident E-field $\vec{\mathcal{E}}_{\text{inc}}$, the backscattered field at the reader can be written as[2]

$$\vec{\mathcal{E}}_{\text{scat}} = \vec{\mathcal{E}}^{\,\text{M}}_{\text{scat}} - \Gamma I_{\text{M}} \frac{\vec{\mathcal{E}}_a}{I_a}, \tag{1}$$

where

- $\vec{\mathcal{E}}^{\,\text{M}}_{\text{scat}}$ is the signal at the reader given current I_{M} passes through Z_A;
- $\Gamma = \frac{Z_L - Z_A^*}{Z_L + Z_A^*}$ is the (complex) reflection coefficient between the antenna and load;
- $I_M = \frac{V_{OC}}{2R_A}$ is the current through Z_A when the antenna and load are conjugate matched $Z_L = Z_A^*$ corresponding to the maximum power transfer condition;
- $\vec{\mathcal{E}}_a / I_a$ is the electric field strength at the reader per unit Ampere of antenna current.

The first (second) term represents the structural (antenna) mode scattering, respectively.

[2]Using Green's decomposition [33][7] of the antenna and structural scattering modes to describe the scattered wave at the receiver.

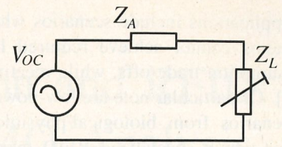


Fig. 3. Thevenin equivalent circuit of an RFID tag. V_{OC} is the voltage induced by the reader's CW, Z_A is the tag antenna's equivalent impedance, and Z_L is the combined impedance of the tag front end and backscatter modulator.

To modulate the backscatter, the tag switches the variable load Z_L between discrete states. For example in Fig. 2, the tag switches the modulator impedance between Z_1 and Z_2 resulting in the corresponding reflection coefficients Γ_1 and Γ_2, respectively. The resulting E-field at the reader's antenna is one of the two signals $\vec{\mathcal{E}}^{\,\text{M}}_{\text{scat}} - \Gamma_1 I_{\text{M}} \frac{\vec{\mathcal{E}}_a}{I_a}$; $\vec{\mathcal{E}}^{\,\text{M}}_{\text{scat}} - \Gamma_2 I_{\text{M}} \frac{\vec{\mathcal{E}}_a}{I_a}$. Demodulating the above signal with the standard quadrature receiver architecture, leads to a complex baseband equivalent signal

$$y = \sqrt{P|\Gamma_{1,2}|^2} e^{-j\phi} x + D + w. \tag{2}$$

The backscatter modulator state determines the (unknown) symbol $x \in \{-1, +1\}$, the offset D results from the (constant) structural scattering (and any CW leakage of the transmit signal into the receiver path) and the additive (complex) white Gaussian noise is $w \sim \mathcal{CN}(0, \sigma^2)$. The $e^{-j\phi}$ term models any random phase rotation of the backscattered symbol resulting from the uplink channel. We assume the reader has a monostatic[3] architecture and the channel state remains coherent over multiple symbol periods, so D and ϕ are effectively constants. Using pilot symbols, the reader estimates D and ϕ in order to shift and de-rotate the constellation [35] as illustrated in Fig. 4. Otherwise, if these components cannot be estimated and compensated for, the reader must use non-coherent detection techniques [36], [34]. For short range and low mobility operation with symbol rates on the order of 100s of Kbaud, it is reasonable to assume a coherent receiver is possible at the reader.[4] The term $P = \frac{|I_{\text{M}} \vec{\mathcal{E}}_a|^2}{8|I_a|^2}$ is a constant that accounts for the path loss between the tag and reader, offset removal, and quadrature down conversion. The detection performance depends on the Euclidean distance between the two reflection coefficients states via $|\Gamma_{1,2}| = |\Gamma_1 - \Gamma_2|$ and the corresponding SNR $= P|\Gamma_{1,2}|^2/\sigma^2$.

It is possible to generalize backscatter to other (2-dimensional) constellations [28] such as a four point constellation shown in Fig. 4. The antenna mode scattering component of (1) is a complex scalar multiple of Γ, which is determined by Z_L. So by choosing Z_L properly, quadrature backscatter modulation can be achieved. To understand the relation between the modulation impedance choice and the resulting constellation points, consider an arbitrary complex constellation alphabet $x_i \in \mathcal{X}$. The corresponding set of Γ_i

[3]Monostatic readers use the same local oscillator (LO) for the transmit and receive chains, and bistatic readers use a seperate LOs. If the LOs are not common, then there is a frequency offset observed at the receiver. [34]

[4]This can be justified by using rule of thumb approximation of channel coherence $\frac{\lambda}{2v}$, λ is wavelength and v is source/destination velocity.

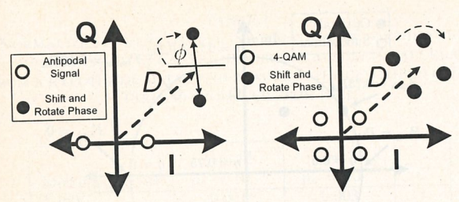


Fig. 4. A binary antipodal constellation and a 4-QAM constellation, D is a constant offset due to structural scattering, and $e^{-j\phi}$ is a random phase rotation of x. Partially reproduced from [24].

values are then [35]

$$\Gamma_i = \alpha \frac{x_i}{\max_{x \in \mathcal{X}} |x|}, \tag{3}$$

where $0 < \alpha \leq 1$ controls the amount of impedance mismatch between the tag's antenna and load. The corresponding impedance load is given by $Z_L = \frac{Z_A^* + \Gamma_i Z_A}{1 - \Gamma_i}$. The demodulated backscatter modulated signal appears as the transmitted constellation $\mathcal{X}$ but with an offset D due to the structural scattering and a phase rotation. Note that this essentially constitutes *one* mapping of constellation symbols to the points Γ_i; which is not necessary unique. Adding a constant offset to all the symbols in $\mathcal{X}$ will result in a different values of Γ_i, but the detection performance of the shifted constellation remains identical, as is well-known. While RFID modulation is still largely confined to binary due to hardware constraints, higher order (4-QAM) modulator designs have been successfully prototyped [35].

B. Coded Modulation for RFID

Backscatter communication remains confined to operation over narrowband channels[5], so higher spectral efficiency will be key to achieving higher data rates. The primary constraint on in backscatter systems is symbol rate: high rates are affected by inter-symbol interference (ISI) and high rates increase the tag's clock frequency. For the former, single carrier systems require complex equalizers at the receiver, and for the latter, increasing the clock frequency increases the tag's energy consumption. While there has been progress towards ultra-wideband (UWB) backscatter systems [37], the primary benefit of UWB is enhanced frequency diversity against fading and not ISI resolution at the receiver. Also, UWB receivers require sophisticated analog processing. Hence, we assume a narrowband coherent Gaussian channel as described by (2).

The purpose of this section is to discuss the energy and rate trade-offs between backscatter constellation designs and error correction codes. While increasing the constellation order improves the spectral efficiency of the backscatter link, the tag pays an additional energy cost due increased impedance between mismatch the tag and antenna. The power harvesting efficiency decreases, because any impedance mismatch decreases the power transfer efficiency between the tag [26]. To quantify the loss in power efficiency, consider the metric

[5]The highest symbol rate in the ISO 18000-6C standard is 640KBaud.

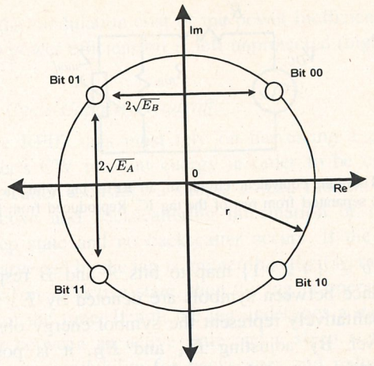


Fig. 5. (a) 4-QAM constellation with $E_A = E_B$. (b) 4-QAM constellation with $E_A > E_B$. Reproduced from [24]

normalized power loss per information bit

$$P_{\text{loss}} = \frac{P_M - P_{\text{back}}}{C\, P_M} \tag{4}$$

where P_M is the maximum amount of power harvested under matched conditions between the tag and antenna. During backscatter operation, the average power harvested is P_{back}. In order to account for the gains of spectral efficiency, the term C is the number of information bits per symbol. Increasing the constellation order will increase the C term, but in turn it will reduce P_{back}. So a system with an uncoded 4 point constellation (2 bits per symbol) will spend half the amount of time in the backscatter state as compared to a system using a binary constellation. Forward error correction (FEC) codes provides a new degree of freedom for a system designer to strike a balance between P_{loss} and the rate achieved.

As a case study to quantify the trade-off between P_{loss} and spectral efficiency, suppose a tag backscatters a general 4-QAM constellation, i.e. an uncoded bit pair (A, B) maps onto a complex symbol x. To simplify analysis, bits A and B map to two orthogonal binary phase shift (BPSK) signals

$$x = \sqrt{E_B} b + j\sqrt{E_A} a \tag{5}$$

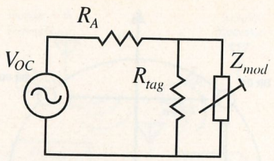


Fig. 6. Thevenin equivalent circuit of an RFID tag with the modulator impedances separated from rest of the tag IC. Reproduced from [24].

where $a, b \in \{+1, -1\}$ map to bits A and B respectively. The distance between symbols are denoted by E_A and E_B, which qualitatively represent the symbol energy observed at the receiver. By adjusting E_A and E_B, it is possible to independently control the uncoded bit error rate of bit A or B, e.g. the respective bit error rates are $\mathcal{Q}(\sqrt{2E_A/N_0})$ and $\mathcal{Q}(\sqrt{2E_B/N_0})$.[6] Choosing $E_A = E_B$ results in the standard quadrature phase shift signal (QPSK) or equal error protection (EEP) for both uncoded bits. As an alternative, $E_A > E_B$ results in a skewed QPSK constellation and unequal error protection (UEP) for both uncoded bits. A graphical example is given in Fig. 5. For a particular link budget example, we will show that a UEP scheme with the appropriate FEC applied exhibits superior performance than EEP.

Assume that the modulator impedance Z_{mod} is placed in parallel to the tag IC with equivalent resistance R_{tag}, and the antenna has equivalent resistance R_A, as shown by the Thevenin circuit in Fig. 6 [26] [22].[7] For a minimum scattering antenna, the information bearing component of the signal at the reader's receiver (1) is proportional to current passing through the tag's antenna port I_A [7],[26], which can be modulated through the modulator impedance state. Not all antennas share the minimum scattering property, so despite choosing $I_A = 0$, a tag's antenna may still produce a non-zero signal at reader [7]. As shown by (1), this additional offset is due the antenna's structural scattering component. Since these are constant offsets, the coherent receiver removes their contribution without any effect on detection performance. Hence for a coherent receiver, the backscattered constellation observed by the reader is effectively proportional to I_A.

Rather than designing constellations directly in terms of Z_{mod}, the antenna current can be shown to proportional to a design variable $\eta \in \mathbb{C}$

$$I_A = \frac{V_{OC}}{R_A}\eta \tag{6}$$

where η is confined to the set $W = \{\eta \in \mathbb{C} : |\eta - 0.75| \leq 0.25\}$. Essentially, the set W defines the feasible backscatter states by the tag. As such η corresponds to Z_{mod} [24] value. By constructing a set of backscatter states $\eta_0, \eta_1, \ldots$, a desired constellation, such as the one depicted in Fig 4, can be constructed.

The power transferred to R_{tag} defines the power available to the tag to harvest P_{tag},

$$P_{\text{tag}} = \frac{1}{2}|I_{\text{tag}}(Z_{\text{mod}})|^2 R_{\text{tag}}, \tag{7}$$

[6] $\mathcal{Q}(x)$ denotes the tail probability of the Gaussian distribution.

[7] This is reasonable if the inductive and capacitive components of antenna and tag IC are tuned out by matching.

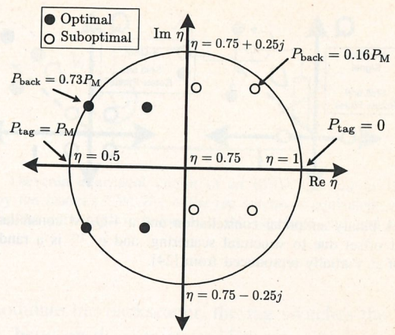


Fig. 7. Two 4-QAM constellation with identical detection error by the reader, but with different P_{back} values. One constellation uses the optimal η values, while the other constellation is arbitrarily placed. The solid-lined circle is the boundary of the set W, the feasible η values. The P_{tag} values are given for the match ($\eta = 0.5$) and short ($\eta = 1$) state. P_{back} is give for the optimal constellation design and for the arbitrarily placed constellation. Reproduced from [24].

and $I_{\text{tag}}(Z_{\text{mod}})$ is the current passing through R_{tag} given a modulator impedance of Z_{mod}. As before, instead of working directly with Z_{mod}, P_{tag} can be written in terms of power harvested in the match state and η [24]

$$P_{\text{tag}} = 4P_{\text{M}}|1 - \eta|^2. \tag{8}$$

Looking at P_{tag} geometrically (Fig. 7 as reference), a circuit designer should place the constellation points closest to the impedance match point ($\eta = 0.5$) in order to maximize the power delivery to the tag.

Returning to our ongoing 4-QAM constellation example, the *average* power harvested during backscatter across all four states η_0 to η_3 (assuming the latter are equiprobable) is

$$P_{\text{back}} = \frac{1}{4}\sum_{i=0}^{3} 4P_{\text{M}}|1 - \eta_i|^2, \tag{9}$$

where η_i maps to symbol state i. The values of η_i are chosen to meet the following optimization[8] criteria: maximize P_{back}, constellation set satisfies some constellation geometry, and a BER specification is satisfied for some link budget [26], [29]. For the constellation given in Fig. 7, the P_{back} values are very different but share the same BER.

The above also explains the motivation in choosing a *rectangular* 4-QAM constellation ($E_A > E_B$) by examining the P_{tag} metric defined by (8) closely. Note that switching between symbols by changing only the real component of η tends to be less efficient in terms of power harvesting than changing the imaginary component of η. For example, consider the following two binary constellations defined by their η values, $\{\eta_0^R = 0.5, \eta_1^R = 0.75\}$ and $\{\eta_0^I = 0.533 + 0.125j, \eta_1^I = 0.533 - 0.125j\}$. Since the euclidean distance of the two sets is equal, $|\eta_0^R - \eta_1^R| = |\eta_0^I - \eta_1^I|$, the error performance is identical. However, $P_{\text{back}} = 0.625P_{\text{M}}$ for the first set and $P_{\text{back}} = 0.93P_{\text{M}}$ for the second set. This suggests that a *rectangular* 4-QAM constellation as shown in Fig. 5(b) is more efficient in terms of harvested power. The

[8] More details on this optimization procedure are given in [24].

TABLE I
NORMALIZED POWER LOSS PER INFORMATION BIT FOR DIFFERENT MODULATIONS AND FECS. THE NUMERICAL RESULT IS CALCULATED FROM A HYPOTHETICAL TAG AND READER SETUP DESCRIBED IN [24]. TABLE REPRODUCED FROM [24].

Modulation Type	P_{loss} at $p_e = 10^{-3}$	P_{loss} at $p_e = 10^{-5}$	C
2-PSK	0.001	0.003	1
UEP $R = 1/4$ $d_{free} = 18$	0.017	0.024	1.25
UEP $R = 1/2$ $d_{free} = 8$	0.021	0.029	1.5
UEP $R = 3/4$ $d_{free} = 5$	0.022	0.031	1.75
EEP $R = 3/4$ $d_{free} = 5$	0.025	0.034	1.5
EEP $R = 1/2$ $d_{free} = 8$	0.03	0.041	1
4-QAM	0.04	0.057	2
2-ASK	0.08	0.11	1

asymmetry in power efficiency marks one of major differences in modulation design between passive backscatter and active transmitter systems.

Traditionally, FEC codes are applied to 4-QAM constellations by coding over both bits such both bits receive equal amounts of protection from the FEC code. Correspondingly, this type of coding scheme gives a rate of $2R$. Instead if only one bit is coded and the other bit is left uncoded, the two bits now have UEP but with an overall rate $1 + R$. To take advantage of the added protection of the FEC code for the EEP, E_A and E_B are reduced in order to decrease the impedance mismatch during the backscatter operation. As consequence, this increases P_{back}. Since only one bit is coded for the UEP case, the ratio between E_A and E_B are chosen such that the BER of the coded bit is approximately equal to the uncoded bit, as illustrated in Fig. 5(b). The method, used by this work, to measure the strength of a FEC code is the following approximation to a BER of a coded BPSK signal [38]

$$p_e \approx \mathcal{Q}\left(\sqrt{2Rd_{free}\frac{E_b}{N_0}}\right) \tag{10}$$

where d_{free} is the minimum free distance between two codewords and E_b is energy per information bit.

Table I provides the P_{loss} values for UEP and EEP constellations with FEC codes with different rates and d_{free} values.[9] To quantify a baseline, examples of uncoded binary phase shift keying (PSK), binary amplitude shift keying (ASK), uncoded 4-QAM are given.[10] The results show that UEP gives higher spectral efficiency and better P_{loss} performance than EEP. Although binary PSK remains the best solution for power efficiency, the UEP is a possible solution to improve the spectral efficiency without paying a higher power cost to the tag. The reasoning being that a powerful (low rate) FEC codes reduces the modulation cost of the power inefficient bit, and the more power efficient bit is left unprotected (high rate).

[9] The rates and d_{free} values are taken from known good convolutional codes [39].

[10] PSK restricts Z_{mod} to have only reactance values and ASK restricts Z_{mod} to have only resistive values.

C. Duty Cycle-Capacity Tradeoff

Passive RFID tags must rely on harvesting a portion of the reader's CW incident energy in order to be operational for backscatter. Consider a simple 2-state model: the tag is either active and backscattering information or the tag is in a sleep state and no backscatter occurs. If the (average) power harvested by the tag is greater than the (average) power consumed in its active state, then the tag is operational 100 percent of the time. If not, the tag undergoes a *duty cycling* behavior between an active state and a sleep state; clearly this reduces *availability* for backscatter and reduces uplink throughput. In this sub-section, we further explore this aspect.

The duty cycle is defined as $D_{\text{cycle}} = T_{\text{A}}/(T_{\text{A}} + T_{\text{S}})$, where T_{A} (T_{S}) are the times spent in the active (sleep) state, respectively. During the sleep state, the tag consumes no energy and the energy harvested with rate P_{M} is stored for use during the active state. During the active state, a) the tag consumes the stored energy at rate P_{C} and b) harvests (average) energy at rate P_{back} as determined by (9). The net rate of energy consumption during backscatter is the difference of the power consumed (P_{C}) and power harvested (P_{back}). Assuming that the energy harvested in the sleep state must equal the energy expended during the active state, the duty cycle can be written in terms of the harvested energy rates

$$D_{\text{cycle}} = \frac{P_{\text{M}}}{P_{\text{M}} + P_{\text{C}} - P_{\text{back}}}. \tag{11}$$

As discussed in the previous section, P_{back} is determined by the constellation design. Note that this model assumes a *linear* relationship between input power and actual usable power. Actual power harvester circuitry results in non-linear effects that are not taken into account here, for the sake of simplicity. Note that measurements from an actual harvester [23] show that the relationship is nearly linear once a certain input power threshold is exceeded, but where this threshold occurs depends on numerous implementation specific details, such as the harvester's architecture and the RF matching network between the harvester and antenna [23]. Accurately modeling these non-linear effects is important for evaluating performance of a specific backscatter system, but is beyond the scope of this work; initial efforts are described within [25].

Consider a binary backscatter modulator where Z_{mod} (as in Fig. 6) has two states Z_1 and Z_2, which are strictly resistive. The modulated symbol rate is fixed to F symbols per second. One modulator state remains in the matched condition (i.e., Z_1 is an open circuit) and the other state has the value Z_2. By varying the value of Z_2 between an open ($Z_2 = \infty$) and short state ($Z_2 = 0$), the harvested power during backscatter P_{back} decreases but link reliability improves. Reliability in terms of link BER is given by

$$p_e = \mathcal{Q}\left(\sqrt{\frac{2P|\Gamma_{1,2}|^2}{\sigma^2}}\right). \tag{12}$$

where the constraints of Z_1 and Z_2 above translate to $|\Gamma_{1,2}| \leq 1$. Using the analysis in [26], P_{back} can be written in terms of

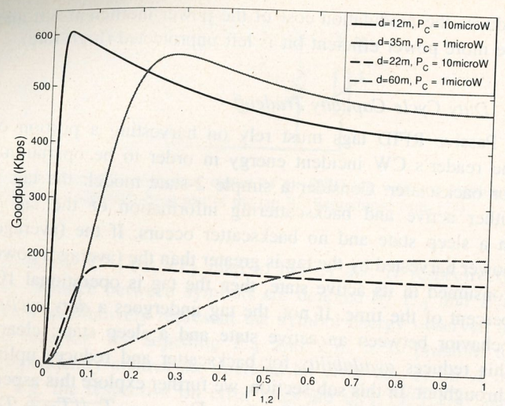


Fig. 8. Goodput vs. $|\Gamma^{1,2}|$ for varying tag-reader distances d and tag power consumption P_C.

$|\Gamma_{1,2}|$.

$$P_{\text{back}} = P_{\text{M}} \frac{1 + (1 - |\Gamma_{1,2}|)^2}{2}. \tag{13}$$

By increasing $|\Gamma_{1,2}|$ the BER improves, but P_{back} and the corresponding tag duty cycle D_{cycle} decreases.

To quantify the tradeoff between link reliability and tag duty cycling, considering the following definition of goodput (G) as a function of $|\Gamma^{1,2}|$

$$G = D_{\text{cycle}} \times C_{\text{BSC}} \times F \tag{14}$$

where C_{BSC} is the capacity of a binary symmetric channel (BSC) with crossover probability p_e (12).[11] G represents the time averaged throughput given that the tag cycles between a sleep state and an active state. Assuming the linear power transfer model, Fig. 8 illustrates how the goodput varies as a function $|\Gamma^{1,2}|$ for different distances between the tag and reader (d), and for different tag IC power consumption P_C. Symbol rate F is fixed to the maximum rate of 640KSymbols/sec, or equivalently 640 Kbps (occurs when $D_{\text{cycle}} = 1$, $C_{\text{BSC}} = 1$). The link budget model and parameters used to calculate the goodput are identical to the model in [26].

The characteristics of the goodput curves can be categorized as either *modulation* limited or *power* limited. The first three curves[12] in Fig. 8 are in the modulation limited regime. Increasing link reliability via $|\Gamma_{1,2}|$ provides only a marginal increase in C_{BSC}, but the decrease in D_{cycle} offsets any capacity gains. To take advantage of the improved link quality, higher order modulation and FEC codes will be required. The last curve[13] represents the power limited regime, because $|\Gamma_{1,2}| = 1$ is required to maximize goodput. In this case, increasing the modulation order will have little impact on the overall goodput, because the communication link capacity is limited more by the transmit power at the reader and not the constellation size. Additionally, the choice of $|\Gamma_{1,2}| = 1$ may be optimal for the power limited case, but for the other scenarios this value of $|\Gamma_{1,2}|$ may result in a goodput that is substantially degraded. This underscores the need for future tags using adaptive modulation and coding schemes that are *aware* of on-tag power harvesting efficiency.

[11]The capacity of a BSC with crossover probability p is defined as $C_{\text{BSC}} = 1 - H(p)$, where $H(p)$ is the Shannon entropy of a Bernoulli random variable with probability p [40].

[12]Corresponding to ($d = 12$m, $P_C = 10\mu$W), ($d = 35$m, $P_C = 1\mu$W), and ($d = 22$m, $P_C = 10\mu$W).

[13]Corresponding to ($d = 60$m, $P_C = 1\mu$W).

III. RFID MIMO Channels

A. Dyadic Backscatter Channel

Current passive tags are limited in range because of their IC power requirements, but as these continue to decrease (due to improvements in circuits and process technology), RFID systems will revert to being uplink limited, as shown in [26]. A driver for this trend is the anticipated use of RFID-like tags in sensor applications that will significantly increase the volume of data sent to a collector node (like a reader). It is well known that link throughput and reliability enhancements over traditional wireless links can be achieved by adding multiple antennas at the two ends, resulting in so-called MIMO systems. For RFID, multiple antennas at the reader can be readily accommodated; of late, tags operating at 5 GHz with multiple antennas have been prototyped[41], [42].[14]

The fading characteristics of a MIMO RFID system differs significantly from normal wireless links operating in far field propagation modes, and to better capture the fading behavior of MIMO RFID channels, the dyadic backscatter channel (DBC) was first introduced by [27]. What distinguishes the DBC model from a standard M transmit, N receive antennas (M, N) Rayleigh MIMO channel is that each tag antenna behaves as a *pinhole* or *keyhole* for the downlink, i.e., all multipath components combine at a single physical point [27]. The *combined signal then re-scatters* [43][44] as if generated from a point source, and propagates to the receive antenna. Pinholes in traditional wide-area (M, N) MIMO systems have also been known to occur in several specific situations as described in [45] and [27]. To motivate the DBC model, the standard MIMO and 'pinhole' MIMO channels are first described.

The received signal $\mathbf{y} \in \mathbb{C}^N$ for a symbol period over a standard (M, N) flat fading MIMO channel is given by [46]

$$\mathbf{y} = \mathbf{H}\mathbf{x} + \mathbf{w} \tag{15}$$

where $\mathbf{H} \in \mathbb{C}^{N \times M}$ is the MIMO channel matrix, $\mathbf{x} \in \mathbb{C}^M$ is the transmitted signal, and $\mathbf{w} \in \mathbb{C}^N$ is AWGN. The receiver has full knowledge of $\mathbf{H}$ through pilot signals, and the transmitter has no knowledge of the channel state. Typically, $\mathbf{H}$ is modeled as a matrix with i.i.d. complex Gaussian entries, reflecting the fact that the numerous scattered paths between any transmit-receiver antennas pair are non-overlapping, resulting in independent Gaussian fading. However in the pinhole MIMO channel, there exists *two* sets of paths traveling to and from each pinhole, hence the channel matrix for L independent pinholes is modeled as a sum of dyadic (outer) products [45]

$$\mathbf{y} = \sum_{i=1}^{L} q_i \mathbf{h^{rx}}_i \mathbf{h^{tx T}}_i \mathbf{x} + \mathbf{w} = \mathbf{H^{rx}} \mathbf{Q} \mathbf{H^{tx T}} \mathbf{x} + \mathbf{w} \tag{16}$$

[14]Multiple antennas on tags operating at lower frequencies, such as the unlicensed 900 MHz band, are impractical today.

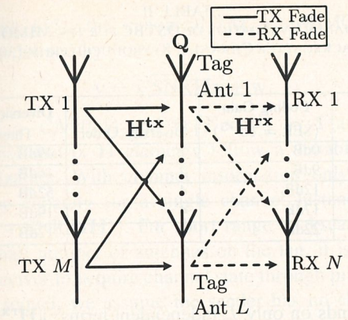


Fig. 9. The (M, L, N) DBC, where the signal observed at each receive antenna is the cascaded of the $\mathbf{H}^{tx}$ and $\mathbf{H}^{rx}$ channels. Each tag antenna behaves as a pinhole, re-scattering the incident CW from the reader. Reproduced from [30].

where $[\mathbf{h^{tx}}_1, \ldots, \mathbf{h^{tx}}_L] = \mathbf{H^{tx}} \in \mathbb{C}^{M \times L}$, $[\mathbf{h^{rx}}_1, \ldots, \mathbf{h^{rx}}_L] = \mathbf{H^{rx}} \in \mathbb{C}^{N \times L}$, $[q_1, \ldots, q_L]^T = \mathbf{q} \in \mathbb{C}^L$, and $\text{diag}\{\mathbf{q}\} = \mathbf{Q} \in \mathbb{C}^{L \times L}$. The matrices $\mathbf{H^{tx}}$ and $\mathbf{H^{rx}}$ represent the channel between the reader transmit antennas and each pinhole, and from the pinhole to the reader receive antennas. $\mathbf{Q}$ represents the complex gain at each pinhole with elements q_i determined by the physical environment that is assumed to remain static. Furthermore, the channel to and from the tag pinholes are assumed flat and independent, whereby each element in $\mathbf{H^{rx}}$ and $\mathbf{H^{tx}}$ are i.i.d $\mathcal{CN}(0, 1)$.

Consider a RFID system consisting of a multi-antenna reader with M transmit antennas and N receive antennas, and a RFID tag with L antennas as in Figure 9. The corresponding (M, L, N) DBC model has the form of (16) [27] but with the following key difference: for the pinhole MIMO channel, the receiver uses the noisy observation of $\mathbf{H^{rx}} \mathbf{Q} \mathbf{H^{tx T}} \mathbf{x}$ to estimate the unknown signal $\mathbf{x}$. For the RFID scenario, the signal $\mathbf{x}$ is a *known CW* generated by the reader; the signal of interest at the reader is instead the elements of $\mathbf{Q}$, which are determined by the tag's impedance loading as discussed in Sec. II. Hence, the receiver uses $\mathbf{H^{rx}} \mathbf{Q} \mathbf{H^{tx T}} \mathbf{x}$ to estimate the the unknown signal $\mathbf{Q}$ with the transmit signal $\mathbf{x}$ known a-priori.[15] By modulating different values of $\mathbf{Q}$, the tag's antenna array can spatially control the backscatter.

In addition to defining the DBC model, [27] analyzed the BER of uncoded BPSK (e.g. $\mathbf{Q} = \pm\mathbf{I}$) over the DBC. Their results provided two interesting insights. First, increasing the number of tag antennas (L) while keeping reader receive antennas $N = 1$ provides SNR gain (upto 8 dB) but no diversity order gain. Second, diversity order gain occurs only by increasing *both* L and N. Comparing these results to the (M, N) Rayleigh channel, it is interesting to note that increasing the number of transmit antennas without space-time codes has no impact on BER for the Rayleigh channel, but for the DBC there exists coding gains.

B. Space-Time Coding in the DBC

As is well-known, space-time coding provides an approach to additional reliability and capacity of wireless systems. The DBC is a relatively new channel model - specifically the fading statistics are different from the standard i.i.d Rayleigh MIMO channels - and has not received much attention from a theoretical perspective. This section will presents recent results from [30] on the pairwise error probability (PEP) and diversity order achievedby orthogonal space time block codes (OSTBC) [47], [48] over DBC.

The base DBC model in (16) represents the system at a single time instant, and needs to be extended over multiple symbol periods to allow for space-*time* analysis. Assume that the reader transmits a CW with equal power ($\mathbf{x} = 1/\sqrt{M}\mathbf{1}_M$) across M transmit antennas successively over K time instants. Then the (M, L, N) DBC model can be for K instants can be written as (for details, see [30])

$$\mathbf{Y} = \sqrt{\text{SNR}} \mathbf{H^{rx}} \mathbf{D^{tx}} \mathbf{S}^a + \mathbf{W} \tag{17}$$

where $\mathbf{S}^a \in \mathbb{C}^{L \times K}$ represents a specific transmitted space-time block codeword (indexed by a) of duration K over L tag antennas. Clearly, each column of $\mathbf{S}^a$ maps to single time instance of $\mathbf{Q}$. The diagonal elements of $\mathbf{D^{tx}} \in \mathbb{C}^{L \times L}$ are distributed as i.i.d. $\mathcal{CN}(0, 1)$; $\mathbf{H^{rx}}$ is defined as before. The $N \times K$ matrix $\mathbf{Y}$ is the signal received by the reader's N receive antennas over the K time instants and $\mathbf{W}$ is AWGN. Under the CW transmit assumption, (17) shows that the DBC is statistically invariant to the number of reader transmit antennas M, i.e. the $(1, L, N)$ channel is equivalent to the (M, L, N) channel even with space-time coding.

Let $\mathbf{S}^a$ be an orthogonal space time block code (OSTBC) codeword that draws from an information symbol vector $\mathbf{c}^a \in \mathbb{C}^K$. The best known OSTBC is the Alamouti code [49], whose codeword (rows denote antennas and columns denote time) is given by

$$\mathbf{S}^a = \begin{pmatrix} c_1^a & -c_2^{a*} \\ c_2^a & c_1^{a*} \end{pmatrix}. \tag{18}$$

The OSTBC scheme transforms the MIMO channel (15) into an equivalent set of SISO AWGN channels parameterized by $\|\mathbf{H}\|_{\mathbf{F}}$ [48], so the equivalent OSTBC channel for the DBC is

$$\mathbf{y}' = \sqrt{\text{SNR}} \|\mathbf{H^{rx}} \mathbf{D^{tx}}\|_{\mathbf{F}} \, \mathbf{c}^a + \mathbf{w}', \tag{19}$$

where $\mathbf{y}' \in \mathbb{C}^K$ is the decoded OSTBC signal at the reader and $\mathbf{w}'$ is AWGN. Using (19), an upper bound for the pairwise error probability between the codewords $\mathbf{S}^a$ and $\mathbf{S}^b$ (denoted by $p(\mathbf{S}^a \to \mathbf{S}^b)$) can be found using the Chernoff bound, and is stated below.

Theorem 1: [30] Assume a (M, L, N) dyadic backscatter channel with constant CW transmit signal across all M antennas and full channel state information (CSI) at the receiver. For an OSTBC, the PEP can be bounded above by

$$p(\mathbf{S}^a \to \mathbf{S}^b) \leq \frac{1}{2} \left(\frac{4}{\text{SNR}} \right)^{LN} \exp\left(\frac{4L}{\text{SNR}} \right) \Gamma\left(1 - N, \frac{4}{\text{SNR}} \right)^L \tag{20}$$

For the diversity order defined as

$$d = \lim_{\text{SNR} \to \infty} \frac{\log p(\mathbf{S}^a \to \mathbf{S}^b)}{\log \text{SNR}}, \tag{21}$$

OSTBCs can achieve $d = L$.

[15]We assume that any leakage of the signal $\mathbf{x}$ from the transmitter to the receiver can be canceled.

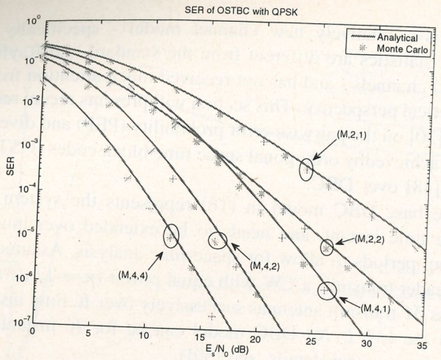


Fig. 10. Analytical bound (20) and Monte Carlo simulations of E_s/N_0 vs SER for OSTBC with QPSK modulation. The channel model simulated is (19), where the receiver has perfect knowledge of the channel state. Reproduced from [30].

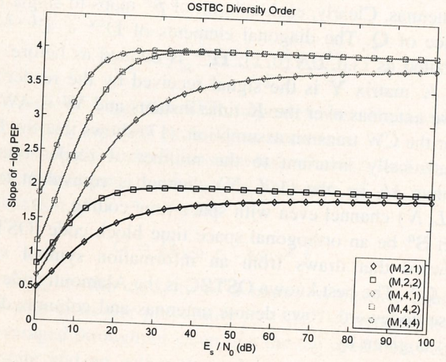


Fig. 11. Slope of $-\log$ PEP for OSTBC with QPSK modulation, i.e. diversity order. The analytical upper bound (20) is used. Reproduced from [30].

Similar to the result for the (M, N) MIMO Rayleigh channel [50], the DBC PEP has an SNR term raised to the negative exponent. Unlike the Rayleigh channel case, however, the DBC bound has a multiplicative component - the upper incomplete Γ function [16], that is increasing in SNR. So as $\text{SNR}^{-LN} \to 0$, $\Gamma\left(1-N, \frac{4}{\text{SNR}}\right) \to \infty$, i.e., the Γ term partially offsets the rate of decrease due to the SNR exponent.

Comparing to the diversity result for the (M, N) Rayleigh, where the maximum diversity is $d = MN$ [50], the DBC diversity order cannot increased beyond L for any space-time code. So *receive antenna diversity at the reader is not beneficial in RFID MIMO over DBC*, i.e., adding additional antennas at the reader has no impact on the asymptotic PEP. Consequently, reliability is best improved by adding antennas to the RFID tag rather than to the reader. Intuitively the diversity order of L makes sense, because there exists only L sets of independent fading paths between the tag and reader, whereas the Rayleigh channel has independent paths between each antenna. To further support this, expanding the matrix norm in the OSTBC channel model (19) illustrates

[16] $\Gamma(s,x) = \int_x^\infty t^{s-1}e^{-t}\mathrm{d}t$.

TABLE II
PERFORMANCE EVALUATION OF OSTBC FOR THE MIMO DYADIC BACKSCATTER CHANNEL. REPRODUCED FROM [30]

Channel	Coding Gain (SER $= 10^{-5}$)	Diversity Order	Diversity Order Threshold
$(M, 2, 1)$	0dB	2	49dB
$(M, 2, 2)$	9dB	2	16dB
$(M, 4, 1)$	12dB	4	52dB
$(M, 4, 2)$	17dB	4	19dB
$(M, 4, 4)$	22dB	4	12dB

that it depends on only L independent terms: $\|\mathbf{H^{rx}D^{tx}}\|_\mathbf{F}^2 = \sum_{i=1}^{L} |D_{ii}^{tx}|^2 \sum_{j=1}^{N} |H_{ij}^{rx}|^2$; the corresponding norm for the Rayleigh channel consists of MN independent terms. While diversity is an asymptotic (in SNR) metric; simulations show that increasing N *does improve system performance* at realistic SNR. Figure 10 plots the analytical bound (20) for QPSK modulated OSTBCs, and the corresponding SER Monte Carlo simulations. The analytical bound corresponds to a pair of QPSK symbols that are nearest neighbors. Figure 11 plots the slope of the analytically derived $-\log(\text{PEP})$ vs E_s/N_0 (energy per information symbol). Table II summarize these performance metrics: coding gain and threshold SNR that achieves 90% of diversity order. Effectively for OSTBC over the DBC, receive antennas N only provides coding gains, while tag antennas L provides additional diversity.

We note that the diversity results described in this section were independently presented in [51]. Additionally, they find the exact error curves for the DBC and show that the diversity order of uncoded MIMO over the DBC is $d = \min(L, N)$. The latter explains the observation in [27] regarding uncoded BER performance; increasing L and N results in diversity order gains, but increasing only L or N does not improve diversity. The next section - on the diversity-multiplexing tradeoff for the DBC - will explain this difference in diversity between the uncoded and OSTBC coded case and explore the benefit of increasing N at the reader.

IV. Diversity Multiplexing Tradeoff for Dyadic Backscatter Channel

A. Background

Unlike the AWGN channel, the wireless fading channel cannot meet arbitrarily low probabilities of error by increasing a code's block length. As such, the ability of any MIMO coding scheme to simultaneously achieve a desired code rate (multiplexing gain) and reliable communications (high diversity order) in a fading channel is bounded by the Diversity-Multiplexing Tradeoff (DMT) [31]. The characterization of the DMT curve is determined by the channel's fading statistics, so it is necessary to recalculate the DMT for new channel fading models. While the DMT for the (M, N) Rayleigh fading channel is fully characterized [31], the corresponding result for the (M, L, N) dyadic backscatter channel is presently unknown, to the best of our knowledge. Using the original problem formulation of the Rayleigh DMT, and results used to characterize the DMT of the double scattering MIMO channel [52], this section characterizes the DMT for the dyadic backscatter channel.

Recalling (15), the canonical (M, N) MIMO Gaussian channel is defined by

$$\mathbf{y} = \sqrt{\text{SNR}}\mathbf{H}\mathbf{x} + \mathbf{w}, \tag{22}$$

where $\mathbf{w} \sim \mathcal{CN}(0, 1)$ and $\text{Tr}\{E[\mathbf{x}\mathbf{x}^\dagger]\} = 1$ and the fading channel matrix $\mathbf{H}$ elements follow a suitable statistical characterization. With channel information only at the receiver, the capacity for a single channel instance of $\mathbf{H}$ is $\log\det(\mathbf{I} + \text{SNR}\,\mathbf{H}\mathbf{H}^\dagger)$. For short range backscatter systems with a small number of antennas on the tag, it is reasonable for the receiver to acquire channel state through pilot symbols.

In the sequel, we assume the sender has no channel state knowledge and the receiver has full channel state knowledge. The sender transmits a codeword with rate $R(\text{SNR})$ and incurs average probability of error $p_e(\text{SNR})$. At high SNR, the performance is quantified by two metrics, multiplexing gain (r) and diversity order (d) [31]

$$\lim_{\text{SNR}\to\infty} \frac{R(\text{SNR})}{\log \text{SNR}} = r \qquad \lim_{\text{SNR}\to\infty} \frac{p_e(\text{SNR})}{\log \text{SNR}} = -d(r) \tag{23}$$

The optimal tradeoff is defined as $d^*(r) = \sup d(r)$, the supremum of the diversity order over all possible schemes achieving a multiplexing gain of r, [31]. In other words, for a system with $R(\text{SNR}) \doteq r \log \text{SNR}$, the corresponding probability of error is no better than $p_e(\text{SNR}) \doteq \text{SNR}^{-d^*(r)}$. The notation $\doteq$ denotes exponential equality, $f(x) \doteq g(x)$ if

$$\lim_{x\to\infty} \frac{\log f(x)}{\log x} = \lim_{x\to\infty} \frac{\log g(x)}{\log x}. \tag{24}$$

So for high SNR, $\text{SNR}^{-d^*(r)}$ is an effective first order approximation for $p_e(\text{SNR})$.[17]

Following the steps first taken by [31], the multiplexing gain is bounded by the ergodic channel capacity [53] of the fast fading MIMO channel

$$\mathcal{C}(\text{SNR}) = E_\mathbf{H}\left[\log\det(\mathbf{I} + \text{SNR}\,\mathbf{H}\mathbf{H}^\dagger)\right]. \tag{25}$$

At high SNR, the ergodic capacity can be approximated by $C(\text{SNR}) \approx \min(M, N)\log\text{SNR}$, and hence $r \leq \min(M, N)$. To achieve the ergodic capacity, a codeword must be averaged over many channel instances, which may not occur in practice with *coherent* narrowband systems. In a slow fading channel, the transmitted codeword experiences a single channel realization, thus the probability that a codeword with rate $r\log\text{SNR}$ is in outage is given by

$$p_{\text{out}}(\text{SNR}) = p\left(\log\det(\mathbf{I} + \text{SNR}\,\mathbf{H}\mathbf{H}^\dagger) < r\log\text{SNR}\right). \tag{26}$$

Corresponding to the diversity order, the outage probability exponent is defined by

$$\lim_{\text{SNR}\to\infty} \frac{\log p_{\text{out}}(\text{SNR})}{\log \text{SNR}} = -d_{\text{out}}(r). \tag{27}$$

For a fixed multiplexing gain r, the relationship between the outage exponent and the diversity order is described next.

As discussed in [31] [52], suppose $\det(\mathbf{I} + \text{SNR}\mathbf{H}\mathbf{H}^\dagger)$ has a pdf $p(\boldsymbol{\alpha})$ defined by a vector $[\alpha_1, \alpha_2, \ldots] = \boldsymbol{\alpha}$. If this pdf has a high SNR approximation

$$p(\boldsymbol{\alpha}) \doteq \text{SNR}^{-\epsilon(\boldsymbol{\alpha})}, \tag{28}$$

[17] The operators $\dot{\leq}$ and $\dot{\geq}$ are defined similarly.

then $p_{\text{out}}(\text{SNR})$ can be approximated by the integral

$$\text{SNR}^{-d_{\text{out}}(r)} \doteq \int_{\mathcal{O}(\boldsymbol{\alpha},r)} \text{SNR}^{-\epsilon(\boldsymbol{\alpha})}\mathrm{d}\boldsymbol{\alpha} \tag{29}$$

over the outage set $\mathcal{O}(\boldsymbol{\alpha}, r)$ such that $\log\det(\mathbf{I}+\text{SNR}\mathbf{H}\mathbf{H}^\dagger) < r\log\text{SNR}$ for a single instance of $\mathbf{H}$. For sufficiently large SNR, $d_{\text{out}}(r)$ can be approximated

$$d_{\text{out}}(r) = \inf_{\mathcal{O}(\boldsymbol{\alpha},r)} \epsilon(\boldsymbol{\alpha}). \tag{30}$$

via Laplace's method [54], as used by [31] [52]. This work assumes that the solution to (30) solves for the corresponding $d_{\text{out}}(r)$ for the DBC.

Note that the outage probability serves as a lower bound to the average probability of error, i.e., $p_{\text{out}}(\text{SNR}) \dot{\leq} p_e(\text{SNR})$, for a codeword with an arbitrary block length K [31]. Block length K is defined as the number of symbols periods required to transmit a space-time codeword, for example, the Alamouti code described by (18) has $K = 2$. For sufficiently large K, $p_{\text{out}}(\text{SNR}) \doteq p_e(\text{SNR})$, hence, $d_{\text{out}}(r) = d^*(r)$.

The remainder of this section are organized as follows. Sec. IV-B calculates the DMT tradeoff function $d_{\text{out}}(r)$. Sec. IV-C derives the block length requirements for $d_{\text{out}}(r) = d^*(r)$ and states the optimal tradeoff curve $d^*(r)$; this is the primary novel contribution of this manuscript. Sec. IV-D discusses how the DMT (an asymptotic metric) correlates with performance in the finite SNR regime.

B. Evaluation of $d_{out}(r)$

The signal model for the (M, L, N) DBC is

$$\mathbf{y} = \sqrt{\text{SNR}}\mathbf{H^{rx}}\mathbf{D^{tx}}\mathbf{x} + \mathbf{w},$$

where $\mathbf{H^{rx}}\mathbf{D^{tx}}$ is defined as in (17). Note that $\mathbf{x}$ is the signal backscattered by the RFID tags. Evaluating the spatial multiplexing gain r is straight forward. The matrix $\mathbf{H^{rx}}\mathbf{D^{tx}}$ has rank equal to $\min(L, N)$ with high probability, so in the high SNR limit the channel capacity [31]

$$\begin{aligned}\mathcal{C}(\text{SNR}) &= E\left[\log\det(\mathbf{I} + \text{SNR}\,\mathbf{D^{tx\dagger}}\mathbf{H^{rx\dagger}}\mathbf{H^{rx}}\mathbf{D^{tx}})\right] \\ &\approx \min(L, N)\log\text{SNR} + \sum_{i=1}^{\min(L,N)} E[\log\lambda_i] \\ &\doteq \min(L, N)\log\text{SNR}\end{aligned} \tag{31}$$

where the $\lambda_1 \geq \lambda_2 \geq \ldots$ are the non-negative ordered eigenvalues of $\mathbf{D^{tx\dagger}}\mathbf{H^{rx\dagger}}\mathbf{H^{rx}}\mathbf{D^{tx}}$. Consequently, the multiplexing gain satisfies $0 \leq r \leq \min(L, N)$ Since the outage probability depends on the statistics of a random matrix, we first provide a necessary definition and lemma relating to random matrices.

Definition 2: Define the $m \times m$ matrix $\mathbf{W} = \mathbf{G}\mathbf{G}^\dagger$ where the columns of $\mathbf{G} \in \mathbb{C}^{m\times n}$ are i.i.d. $\mathcal{CN}(0, \boldsymbol{\Sigma})$ vectors. Then $\mathbf{W}$ follows the Wishart distribution $\mathcal{W}_m(n, \boldsymbol{\Sigma})$ [55].

Lemma 3: [55] [52] Suppose $\mathbf{W} \sim \mathcal{W}_m(n, \boldsymbol{\Sigma})$. Define $a_1 \geq a_2 \geq \ldots \geq a_q \geq 0$ as the non-negative, ordered eigenvalues of $\mathbf{W}$ where $q = \min(m, n)$. Define $b_1 \geq b_2 \geq \ldots \geq b_m \geq 0$ as the ordered eigenvalues of $\boldsymbol{\Sigma}$. For $n \geq m$, the joint pdf $p(\mathbf{a})$ of the ordered eigenvalues of $\mathbf{W}$ is given by

$$K_{m,n}\text{Det}\left[e^{-a_j/b_i}\right]_{i,j} \prod_{i=1}^{m} b_i^{m-n-1}a_i^{n-m} \prod_{i<j}^{m} \frac{a_i - a_j}{b_i - b_j} \tag{32}$$

and $p(\mathbf{a})$ for $m > n$

$$J_{m,n}\mathrm{Det}(\Xi)\prod_{i<j}^{m}\frac{1}{b_i-b_j}\prod_{i<j}^{n}(a_i-a_j) \tag{33}$$

with Ξ

$$\begin{bmatrix} 1 & b_1 & \dots & b_1^{m-n-1} & \frac{b_1^{m-n-1}}{\exp(a_1/b_1)} & \cdots & \frac{b_1^{m-n-1}}{\exp(a_n/b_1)} \\ \vdots & \vdots & \ddots & \vdots & \vdots & \ddots & \vdots \\ 1 & b_m & \dots & b_m^{m-n-1} & \frac{b_m^{m-n-1}}{\exp(a_1/b_m)} & \cdots & \frac{b_1^{m-n-1}}{\exp(a_n/b_m)} \end{bmatrix}$$

$K_{m,n}$ and $J_{m,n}$ are normalizing (positive) constants. Observe that the joint distribution of $\mathbf{a}$ depends only on the eigenvalues $\mathbf{b}$ of $\mathbf{\Sigma}$.

Following the analysis used by [31], the outage probability of the DBC is

$$p(\log\det(\mathbf{I}+\mathrm{SNR}\,\mathbf{D^{tx\dagger}H^{rx\dagger}H^{rx}D^{tx}}) < r\log\mathrm{SNR}). \tag{34}$$

Using well-known results for the matrix determinant -

$$\det(\mathbf{I}+\mathrm{SNR}\,\mathbf{D^{tx\dagger}H^{rx\dagger}H^{rx}D^{tx}}) = \prod_{i=1}^{\min(L,N)}(1+\mathrm{SNR}\lambda_i), \tag{35}$$

where λ_i is defined as before. Using the method described by [31], the eigenvalues of the channel matrix related to the outage probability for a given spatial multiplexing gain. Assume $\alpha_i = -\log\lambda_i/\log\mathrm{SNR}$, so that $\lambda_i = \mathrm{SNR}^{-\alpha_i}$ and $\alpha_1 \le \alpha_2 \le \dots$. Each product term in the determinant can be written as $1+\lambda_i\mathrm{SNR} \doteq \mathrm{SNR}^{(1-\alpha_i)^+}$ where $(x)^+ = \max(0,x)$. The outage probability in the high SNR regime is approximated by

$$p_{\mathrm{out}}(\mathrm{SNR}) \approx p\left(\prod_{i=1}^{\min(L,N)}\mathrm{SNR}^{(1-\alpha_i)^+} < \mathrm{SNR}^{r}\right). \tag{36}$$

Define $\mathcal{A} = \{\boldsymbol{\alpha} | \sum_{i=1}^{\min(L,N)}(1-\alpha_i)^+ < r, \alpha_1 \le \alpha_2 \le \dots\}$ as the set of $\boldsymbol{\alpha}$ that cause an outage and $p(\boldsymbol{\alpha})$ as the joint pdf of the eigenvalues λ_i under the change of variables to α_i. The outage probability is given by the integral

$$p_{\mathrm{out}}(\mathrm{SNR}) = \int_{\mathcal{A}} p(\boldsymbol{\alpha})\mathrm{d}\boldsymbol{\alpha}. \tag{37}$$

Evaluating the above integral in closed form is difficult because the distribution $p(\boldsymbol{\alpha})$ is unknown. Similar to the work on DMT of the double scattering channel [52], it is easier to find a joint distribution $p(\boldsymbol{\alpha},\boldsymbol{\beta})$, whose pdf can be expressed in closed form, and solve for (37) over both $\boldsymbol{\alpha}$ and $\boldsymbol{\beta}$, which avoids the explicit calculation of $p(\boldsymbol{\alpha})$.

For a fixed $\mathbf{D^{tx}}$ and random $\mathbf{H^{rx\dagger}}$, the columns of $\mathbf{G} = \mathbf{D^{tx\dagger}H^{rx\dagger}}$ are iid Gaussian vectors with the correlation matrix $\mathbf{D^{tx}D^{tx\dagger}}$. Therefore $\mathbf{GG^\dagger}$, for fixed $\mathbf{D^{tx}}$, generates a Wishart matrix (defn. 2) with distribution $\mathcal{W}_L(N, \mathbf{D^{tx}D^{tx\dagger}})$, and $p(\boldsymbol{\lambda}|\mathbf{D^{tx}})$ follows the distribution of the eigenvalues of a Wishart matrix given by lemma 3.

Define the ordered eigenvalues of $\mathbf{D^{tx}D^{tx\dagger}}$ as $\mu_1 > \mu_2 > \dots > \mu_L > 0$. Let $\beta_i = -\log\mu_i/\log\mathrm{SNR}$, then $p(\boldsymbol{\alpha}|\boldsymbol{\beta}) \sim \mathcal{W}_L(N, \mathbf{D^{tx}D^{tx\dagger}})$ under the proper change of variables. Combining the known results on the distribution of $p(\boldsymbol{\alpha}|\boldsymbol{\beta})$ [52] and deriving the distribution of $p(\boldsymbol{\beta})$, the joint distribution $p(\boldsymbol{\alpha},\boldsymbol{\beta})$ can be expressed in closed form. Using Bayes rule, the outage probability (37) is equivalently written as [52]

$$p_{\mathrm{out}}(\mathrm{SNR}) = \int_{\mathcal{A}\cap\mathcal{B}} p(\boldsymbol{\alpha},\boldsymbol{\beta})\mathrm{d}\boldsymbol{\beta}\mathrm{d}\boldsymbol{\alpha}. \tag{38}$$

where $\mathcal{B} = \{\beta_1 \le \dots \le \beta_L\}$. (30) will be used to approximate this integral in the high SNR regime. Next we find $\epsilon(\boldsymbol{\alpha},\boldsymbol{\beta})$ such that $p(\boldsymbol{\alpha},\boldsymbol{\beta}) \doteq \mathrm{SNR}^{-\epsilon(\boldsymbol{\alpha},\boldsymbol{\beta})}$.

Since $\mathbf{D^{tx}D^{tx\dagger}}$ is diagonal matrix, the eigenvalues equal the diagonal elements. Each element, $D_{ii}^{tx}D_{ii}^{tx*}$ follows the exponential distribution with parameter 1 and are iid, so the ordered eigenvalue distribution is

$$p(\boldsymbol{\mu}) = L!\exp\left[-\sum_{i=1}^{L}\mu_i\right], \tag{39}$$

and under a change of variables, the high SNR approximation to the pdf in terms of $\boldsymbol{\beta}$ is

$$p(\boldsymbol{\beta}) \doteq \mathrm{SNR}^{-\sum_{i=1}^{L}\beta_i} \tag{40}$$

for all non-negative, i.e. $\beta_i \ge 0$, otherwise $p(\boldsymbol{\beta}) \to 0$ exponentially.

$d_{out}(r)$ - $N \ge L$ Case:

Lemma 4: For $N \ge L$, the joint distribution $p(\boldsymbol{\alpha},\boldsymbol{\beta})$ has the high SNR approximation

$$p(\boldsymbol{\alpha},\boldsymbol{\beta}) \doteq \mathrm{SNR}^{\sum_{i=1}^{L}-(L-N)\beta_i-(N-L+1)\alpha_i} \cdot \mathrm{SNR}^{\sum_{i=1}^{L}-(L-i)(\alpha_i-\beta_i)}\mathrm{SNR}^{\sum_{i<j}^{L}-(\alpha_i-\beta_j)^+} \tag{41}$$

if $\alpha_i \ge \beta_i, \boldsymbol{\alpha} \ge 0, \boldsymbol{\beta} \ge 0$ - otherwise $p(\boldsymbol{\alpha},\boldsymbol{\beta})$ decays to zero exponentially.

Proof: See Appendix A. ∎

Since (41) decays exponentially if the constraints in lemma 4 are not met, that range of values can be excluded from the outage integrand (38) without affecting its high SNR approximation [31][52]; this reduces the sets $\mathcal{A}$ and to $\mathcal{B}$ to $\mathcal{A}' = \{\boldsymbol{\alpha} | \sum_{i=1}^{L}(1-\alpha_i)^+ < r, 0 \le \alpha_1 \le \dots \le \alpha_L\}$ and $\mathcal{B}' = \{\boldsymbol{\beta} | \forall i,\ \beta_i \le \alpha_i,\ \beta_1 \le \dots \le \beta_L,\ \beta_i \ge 0\}$, respectively. Using (41), we may write $p(\boldsymbol{\alpha},\boldsymbol{\beta}) \doteq \mathrm{SNR}^{-\epsilon(\boldsymbol{\alpha},\boldsymbol{\beta})}$ where

$$\epsilon(\boldsymbol{\alpha},\boldsymbol{\beta}) = \sum_{i=1}^{L}(i-N)\beta_i + (N+1-i)\alpha_i + \sum_{i<j}^{L}(\alpha_i-\beta_j)^+, \tag{42}$$

Using (30) the outage probability (38) is evaluated by $\mathrm{SNR}^{-d_{\mathrm{out}}(r)}$, where the exponent $d_{\mathrm{out}}(r)$ is obtained as the result of the following optimization

$$d_{\mathrm{out}}(r) = \inf_{\mathcal{O}(\boldsymbol{\alpha},\boldsymbol{\beta},r)} \epsilon(\boldsymbol{\alpha},\boldsymbol{\beta}) \tag{43}$$

and $\mathcal{O}(\boldsymbol{\alpha},\boldsymbol{\beta},r) = \mathcal{A}'\cap\mathcal{B}'$. Observe that $\epsilon(\boldsymbol{\alpha},\boldsymbol{\beta})$ is decreasing for increase in β_i, and recall that $\beta_i \le \alpha_i$. So for any $\boldsymbol{\alpha}$, $\epsilon(\boldsymbol{\alpha},\boldsymbol{\beta})$ is minimized by choosing $\beta_i = \alpha_i$. Rewriting the optimization in terms of only $\boldsymbol{\alpha}$ yields

$$d_{\mathrm{out}}(r) = \inf\sum_{i=1}^{L}\alpha_i$$

$$\text{subject to: } \sum_{i=1}^{L}(1-\alpha_i)^+ < r,\ \ 0 \le \alpha_1 \le \dots \le \alpha_L \tag{44}$$

The minimum occurs when $\sum_{i=1}^{L}(1-\alpha_i)^+ = r$, or equivalently $L - r = \sum_{i=1}^{L}\alpha_i$ given $0 \le \boldsymbol{\alpha} \le 1$. The corresponding outage exponent is

$$d_{\mathrm{out}}(r) = L - r. \tag{45}$$

$d_{out}(r)$ - $L > N$ Case:

We employ the same strategy as the $N \ge L$ case to find $d_{\mathrm{out}}(r)$.

Lemma 5: For $L > N$, the joint distribution $p(\boldsymbol{\alpha},\boldsymbol{\beta})$ has the high SNR approximation

$$p(\boldsymbol{\alpha},\boldsymbol{\beta}) \doteq \mathrm{SNR}^{-\sum_{i=1}^{N+1}(L-N-1)\beta_i}\mathrm{SNR}^{-\sum_{i=1}^{L}\beta_i}\mathrm{SNR}^{-\sum_{i=1}^{N}\alpha_i} \cdot \mathrm{SNR}^{-\sum_{i=N+2}^{L}(L-i)\beta_i}\mathrm{SNR}^{\sum_{i<j}^{L}\beta_i}\mathrm{SNR}^{-\sum_{i<j}^{N}\alpha_i} \cdot \mathrm{SNR}^{-\sum_{i<j}^{N}(\alpha_j-\beta_i)^+}\mathrm{SNR}^{-\sum_{i=1}^{N}\sum_{N+1}^{L}(\alpha_i-\beta_j)^+} \tag{46}$$

if $\forall 1 \le i \le N,\ \alpha_i \ge \beta_i,\ \boldsymbol{\alpha} > 0,\ \boldsymbol{\beta} > 0$ - otherwise $p(\boldsymbol{\alpha},\boldsymbol{\beta})$ decays to zero exponentially.

Proof: See Appendix B. ∎

Since (46) decays exponentially if the constraints in lemma 5 are not met, that range of values can be excluded from the outage integrand (38) without affecting its high SNR approximation - reducing the sets $\mathcal{A}$ and to $\mathcal{B}$ to $\mathcal{A}' = \{\boldsymbol{\alpha} | \sum_{i=1}^{L}(1-\alpha_i)^+ < r, 0 \le \alpha_1 \le \dots \le \alpha_N\}$ and $\mathcal{B}' = \{\boldsymbol{\beta} | \forall 1 \le i \le N,\ \beta_i \le \alpha_i,\ \beta_1 \le \dots \le \beta_L,\ \beta_i \ge 0\}$.

As before, the terms in the exponent of (46) in lemma 5 can be expressed as the function

$$\epsilon(\boldsymbol{\alpha},\boldsymbol{\beta}) = \sum_{i=1}^{N}(N-i+1)\alpha_i + \sum_{i=1}^{N+1}(i-N)\beta_i + \sum_{i=N+2}^{L}\beta_i + \sum_{i<j}^{N}(\alpha_i-\beta_j)^+ + \sum_{i=1}^{N}\sum_{j=N+1}^{L}(\alpha_i-\beta_j)^+ \tag{47}$$

$d_{\mathrm{out}}(r)$ is given by the solution to the optimization problem (43) over the outage set $\mathcal{O}(\boldsymbol{\alpha},\boldsymbol{\beta},r) = \mathcal{A}'\cap\mathcal{B}'$. To solve this optimization problem, first, find the $\boldsymbol{\beta}$ that minimizes $\epsilon(\boldsymbol{\alpha},\boldsymbol{\beta})$ for any fixed $\boldsymbol{\alpha}$, and finally, solve for the optimal $\boldsymbol{\alpha}$.

The components of $\epsilon(\boldsymbol{\alpha},\boldsymbol{\beta})$ that depend on $\boldsymbol{\beta}' = [\beta_{N+1},\dots,\beta_L]^{\mathrm{T}}$ are

$$\sum_{i=N+1}^{L}\beta_i + \sum_{i=1}^{N}\sum_{j=N+1}^{L}(\alpha_i-\beta_j)^+. \tag{48}$$

For any $\boldsymbol{\alpha}$, it will be shown that $\boldsymbol{\beta}' = \alpha_N\mathbf{1}_{L-N}$ minimizes the above.[18] Suppose $\beta_L \le \alpha_N$, then the contribution of the β_L terms to (48) is

$$\beta_L + \sum_{i=1}^{N}(\alpha_i-\beta_L)^+, \tag{49}$$

otherwise for $\beta_L > \alpha_N$, the above reduces to β_L. To minimize the above it is necessary that $\sum_{i=1}^{N-1}(\alpha_i-\beta_L)^+ = 0$, and due to the ordering of α_i, $\beta_L = \alpha_N$ is the minimization solution. The same logic can be recursively applied to $\beta_{L-1},\dots,\beta_{N+1}$ to show that $\boldsymbol{\beta}' = \alpha_N\mathbf{1}_{L-N}$ is sufficient to minimize (48).

[18] $\mathbf{1}_N$ represents an all 1 column vector with dimension N.

Substituting $\boldsymbol{\beta}' = \alpha_N\mathbf{1}_{L-N}$ back into the original equation results in

$$\epsilon(\boldsymbol{\alpha},\beta_1,\dots,\beta_N) = \sum_{i=1}^{N}(N-i+1)\alpha_i + (L-N)\alpha_N + \sum_{i=1}^{N}(i-N)\beta_i + \sum_{i<j}^{N}(\alpha_i-\beta_j)^+ \tag{50}$$

As in $N \ge L$ case, ϵ is decreasing in increasing β_i. Therefore, choose $\alpha_i = \beta_i,\ \forall 0 < i \le N$. The reduced minimization problem in terms of only $\boldsymbol{\alpha}$ is now

$$d_{\mathrm{out}}(r) = \inf\sum_{i=1}^{N-1}\alpha_i + (L-N+1)\alpha_N$$

$$\text{Subject to: } \sum_{i=1}^{N}(1-\alpha_i)^+ < r,\ \ 0 \le \alpha_1 \le \dots \le \alpha_N \tag{51}$$

In the objective, the term with the largest coefficient (α_N) should be minimized first before reducing the remaining terms. To satisfy the ordering constraints of α_i while minimizing α_N, it is necessary to set $\alpha_i = \alpha_N \forall i \in [1, N-1]$. Setting $\forall i\ \alpha_i = a$, a dummy variable where $0 < a$, the objective is minimized when the constraints are met with equality i.e. $N(1-a)^+ = r$. The corresponding solution is

$$d_{\mathrm{out}}(r) = L(1-r/N). \tag{52}$$

C. DBC DMT

Codeword Length Considerations:

The $d_{\mathrm{out}}(r)$ serves as an upper bound to the optimal tradeoff $d^*(r)$. To show that $d_{\mathrm{out}}(r) = d^*(r)$ for certain cases, we apply the union bound method used by [31] in the Rayleigh DMT calculation. The error event can be expressed as the union of two exclusive events

$$p_e = p(\mathrm{error}|\mathrm{outage})p_{\mathrm{out}} + p(\mathrm{error\ and\ no\ outage}), \tag{53}$$

Since the goal is to prove $p_e \doteq p_{\mathrm{out}}$, consider the following upper bound

$$p_e \le p_{\mathrm{out}} + p(\mathrm{error\ and\ no\ outage}). \tag{54}$$

An error occurs from either the channel being in outage or the additive noise causes an error despite the channel not being in outage. The latter can be driven to an arbitrarily small value by extending a code's block length towards infinity, however, for a finite block length, $p(\mathrm{error,\ no\ outage})$ may dominate the outage probability p_{out}.

Since an outage event does not occur, i.e. $\log\det(\mathbf{I} + \mathrm{SNR}\mathbf{HH}^\dagger) > r\log\mathrm{SNR}$, the multiplexing gain is constrained by $r > \sum_i(1-\alpha_i)^+$. Define the no outage set as $\mathcal{A}'' = \{\boldsymbol{\alpha} | \sum_{i=1}^{L}(1-\alpha_i)^+ > r, 0 < \alpha_1 \le \dots \le \alpha_{\min(L,N)}\}$, similar to the definition of $\mathcal{A}'$. Using the joint distribution of $p(\boldsymbol{\alpha},\boldsymbol{\beta})$, the $p(\mathrm{error\ and\ no\ outage})$ is bounded by [31]

$$p(\mathrm{error\ and\ no\ outage}) \dot{\le} \int_{\mathcal{A}''\cap\mathcal{B}'}\mathrm{SNR}^{-\epsilon(\boldsymbol{\alpha},\boldsymbol{\beta})}\mathrm{SNR}^{-K[\sum(1-\alpha_i)^+-r]}\mathrm{d}\boldsymbol{\beta}\mathrm{d}\boldsymbol{\alpha} \tag{55}$$

As in [31], this integral is evaluated using (30), by finding the $\boldsymbol{\alpha}, \boldsymbol{\beta}$ that minimize the exponent given that the channel state is such that the system is not in outage, i.e.

$$d_{\mathrm{U}}(r) = \inf \ \epsilon(\boldsymbol{\alpha}, \boldsymbol{\beta}) + K[\sum_i (1-\alpha_i)^+ - r]$$

$$\text{Subject to: } \alpha_i \geq \beta_i; \ \ 0 \leq \alpha_1 \leq \alpha_2 \leq \ldots$$

$$0 \leq \beta_1 \leq \beta_2 \leq \ldots; \quad \sum_{i=1}^{\min(L,N)} (1-\alpha_i)^+ > r \tag{56}$$

As before, this optimization can be written in terms of only $\boldsymbol{\alpha}$ by finding the optimal $\boldsymbol{\beta}$ terms first.

Case $N \geq L$, the minimization

$$\inf \sum_{i=1}^{L} \alpha_i + K[\sum_{i=1}^{L} (1-\alpha_i)^+ - r] \tag{57}$$

subject to the constraints in (56). If $K \geq 1$, then the minimum occurs when $\sum_{i=1}^{L}(1-\alpha_i)^+ - r = 0$. Therefore $d_{\mathrm{U}}(r) = L - r$, i.e. the same solution as the outage exponent (45).

Case $L \geq N$, we have

$$\inf \sum_{i=1}^{N-1} \alpha_i + (L-N+1)\alpha_N + K[\sum_{i=1}^{N} (1-\alpha_i)^+ - r] \tag{58}$$

subject to the constraints in (56). If $K \geq \lceil L/N \rceil$, then the minimum occurs when $\sum_{i=1}^{N}(1-\alpha_i)^+ - r = 0$, which gives the same solution as the outage exponent (52).

Returning to the upper bound on error probability (54) it can be seen that if the code block length K meets the above constraints, then the upper and lower bounds are tight, per below:

$$p_e(r) \dot{\leq} \mathrm{SNR}^{-d_{\mathrm{out}}(r)} + \mathrm{SNR}^{-d_{\mathrm{U}}(r)} \doteq \mathrm{SNR}^{-d_{\mathrm{out}}(r)} \tag{59}$$

since $d_{\mathrm{out}}(r) = d_{\mathrm{U}}(r)$. Hence, the probability of error can be upper and lower bounded by $d_{\mathrm{out}}(r)$, which proves $d^*(r) = d_{\mathrm{out}}(r)$. Our desired result is summarized in the following theorem 6. Note that the code length constraint must be met for $d^*(r) = d_{\mathrm{out}}(r)$.

Main Result and Discussion:

Theorem 6: For a (M, L, N) dyadic backscatter channel with code length K, the optimal DMT curve $d^*(r)$ is given by the linear function

- $N \geq L$ and $K \geq 1$

$$d^*(r) = L - r, \quad 0 < r \leq L \tag{60}$$

- $N < L$ and $K \geq \lceil L/N \rceil$

$$d^*(r) = L(1 - r/N), \quad 0 < r \leq N \tag{61}$$

Proof: The diversity order exponent $d_{\mathrm{out}}(r)$ is derived, for both cases, in Sec IV-B at (45) and (52). The argument posed by (59) establishes the block length restrictions such that $d_{\mathrm{out}}(r) = d^*(r)$. ■

Fig. 12 illustrates the tradeoff for the two cases, and as comparison, it plots the Rayleigh DMT for a system with the same antenna configuration. Effectively, the DBC DMT is a linear function connecting the points L and $\min(N, L)$ on the $d(r)$ and r axises. For comparison, the (L, N) Rayleigh

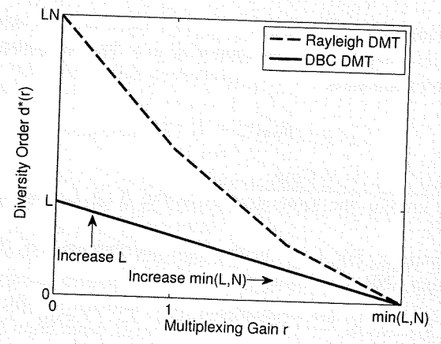


Fig. 12. (M, L, N) DBC and (L, N) Rayleigh Channel Diversity Multiplexing Tradeoff - the curves are plotted for $L = 5, N = 3$.

channel DMT is characterized by the piece-wise linear function with the corner points as $d^*(r) = (L-r)(N-r)$ for integer values of r; see theorem 2 of [31]. The results reveals some interesting new characteristics - while the PEP bounds and diversity order results in Sec III suggest that an increase in receive antennas N has no asymptotic benefits, the DMT proves this is not the case. First for $N < L$, increasing N has multiple effects. It improves the maximum multiplexing gain while increasing the reliability $d^*(r)$ for $0 < r < N$. So while the diversity for $r = 0$ remains unchanged, it improves for all other r. Additionally, increasing N reduces the length of the space-time code required to achieve the optimal DMT. This explains why diversity gains are feasible in the DBC without any space-time codes, because for $N \geq L$, coding only over space (antennas) is sufficient to achieve the optimal $d^*(r)$. These results agree with prior work [51] that reports a maximum diversity of $\min(N, L)$ for space only codes - for $L > N$ a (M, L, N) system cannot have worse performance than a (M, N, N) system.

Increasing N beyond L appears to only have a minor impact in system performance; diversity or spatial multiplexing gains remain bounded by L. This is in clear contrast to the Rayleigh fading channel, where increasing N provides substantial diversity order gains (up to LN) for small values of r. While the DBC can offer the same range of multiplexing gains as the Rayleigh channel, the DBC lacks capability to offer the same level of reliability. Essentially, the DBC is more likely to encounter deeper fades than its Rayleigh counterpart. These DMT results suggest that a system with $L = N$ will strike a balance in performance (diversity and multiplexing) and complexity/cost.

Lastly, the case for which $d^*(r)$ is not solved for is $L > N$ with $K < \lceil L/N \rceil$ - we highlight this as a case that will not occur commonly in practice. Due to space constraints on a RFID tag, it is unlikely for $L > N$ to occur in most situations, and the code length constraint remains small for any practical occurrence of $L > N$. This characteristic is different than (M, N) Rayleigh case, where the code length increases as $M + N - 1$ [31]. So deriving the remaining case for $d^*(r)$ may not offer much practical guidance in choosing L and N.

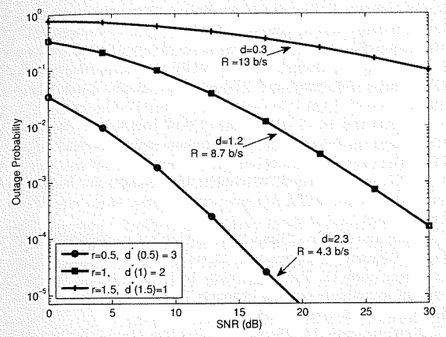


Fig. 13. Monte carlo evaluation of (63) for the $(M, 4, 2)$ DBC. The slope of the diversity curve and $r \log(1 + g\mathrm{SNR})$ is evaluated at 17.1dB for different multiplexing gains r, and the corresponding optimal DMT is denoted by $d^*(r)$.

D. DBC DMT - Finite SNR Regime

While the DMT is originally defined as an asymptotic metric, it is still useful to quantify the behavior of the multiplexing and diversity order gains at *realistic* values of SNR. Existing work [56] on the Rayleigh and Rician MIMO fading channels derive a practical lower bound to the outage probability with respect to the multiplexing gain. Coupled with simulations to verify the bound, these results indicate a significant gap between the asymptotic DMT curve and what can be achieved in practice. This section builds on the results of [56] and formulates the finite SNR DMT for the DBC and provides results derived from simulations, however, developing a closed form to the lower bound is outside of the scope of this manuscript.

The multiplexing gain and diversity order have the following corresponding metrics in finite SNR:

$$r = \frac{R(\mathrm{SNR})}{\log(1 + g\mathrm{SNR})} \qquad d(r, \mathrm{SNR}) = -\frac{\partial \log p_{\mathrm{out}}(\mathrm{SNR})}{\partial \log \mathrm{SNR}}. \tag{62}$$

For small SNR, $\det \log(\mathbf{I} + \mathrm{SNR}\mathbf{H}\mathbf{H}^\dagger) \approx \log(1 + \mathrm{SNR}\|\mathbf{H}\|_F^2)$, so a fair value to choose for the array gain is $g = E[\|\mathbf{H}\|_F^2] = LN$ [56]. The outage probability is redefined slightly,

$$p(\det \log(\mathbf{I} + \mathrm{SNR}\mathbf{H}\mathbf{H}^\dagger) < r \log(1 + g\mathrm{SNR})), \tag{63}$$

in order to account for the new definition of multiplexing gain.

Monte Carlo evaluations of (63) over a range of SNR and for various r represent the main new contributions of this section. Fig. 13 plots the outage probability for the $(M, 4, 2)$ DBC for various multiplexing gains r. Similar to the Rayleigh case [56], only a fraction of the diversity order is achievable at reasonable SNR, and the diversity order worsens as the multiplexing gain is increased. So to achieve high spectral efficiency with high reliability, backscatter communication will require significant time or frequency diversity; both of which may be a challenge for narrow band backscatter systems. Lastly, these results confirm the conclusion of the asymptotic DMT analysis - that DBC is primarily limited by reliability (vulnerability to fading) rather than code rate (multiplexing gain).

V. Conclusion

Despite being demonstrated for over 35 years [57], backscatter communication has been relatively overlooked by the communication theory community. The primary objective of this paper was to emphasize the relevance of passive backscatter as an emerging area for a new class of low-power wireless sensor networks. In particular, we highlight the coupling of coding and modulation with power harvesting for passive backscatter, that presents unique results and design insights vis-a-vis traditional active communication. Additionally, the physical principle behind backscatter communication induces a new channel fading model - the dyadic backscatter channel. We used this channel model to derive new diversity-multiplexing tradeoffs, that are again distinct from those for the well-known Rayleigh fading MIMO channels.

Appendix A
Proof of Lemma 4

Following [31][52], recall that $p(\boldsymbol{\alpha}|\boldsymbol{\beta})$ follows the Wishart eigenvalue distribution defined by (32) for the $N \geq L$, under the change of variables $a_i = \mathrm{SNR}^{-\alpha_i}$ and $b_i = \mathrm{SNR}^{-\beta_i}$. The RHS product term in (32) approximates to

$$\prod_{i<j}^{L} \frac{(\mathrm{SNR}^{-\alpha_i} - \mathrm{SNR}^{-\alpha_j})}{(\mathrm{SNR}^{-\beta_i} - \mathrm{SNR}^{-\beta_j})} \doteq \mathrm{SNR}^{-\sum_{i<j}^{L}(\alpha_i - \beta_i)} \tag{64}$$

due to the identity $\mathrm{SNR}^{-\alpha_i} - \mathrm{SNR}^{-\alpha_j} \doteq \mathrm{SNR}^{-\alpha_i}$ for $\alpha_i < \alpha_j$ [52]. Due to lemma 1 in [52], the determinant term in (32) approximates to

$$\exp\left[-\sum_{i=1}^{L} \mathrm{SNR}^{-(\alpha_i - \beta_i)}\right] \mathrm{SNR}^{-\sum_{i<j}^{L}(\alpha_i - \beta_j)^+} \tag{65}$$

for $\alpha_i \geq \beta_i, \ \forall i$; otherwise $\mathrm{Det}[\exp(-\mathrm{SNR}^{-(\alpha_j - \beta_i)})] \to 0$ exponentially in SNR. Combining all the terms in (32) and $p(\boldsymbol{\beta})$ in (40) gives the form stated in the lemma.

Appendix B
Proof of Lemma 5

Following [31][52], recall that $p(\boldsymbol{\alpha}|\boldsymbol{\beta})$ follows the Wishart eigenvalue distribution defined by (33) for the $N < L$. Performing a change of variables $a_i = \mathrm{SNR}^{-\alpha_i}$ and $b_i = \mathrm{SNR}^{-\beta_i}$, the RHS product terms are approximated in the same fashion as the $N \geq L$ case. Applying lemma 2 in [52], the determinant term is approximated as

$$\begin{aligned}\mathrm{Det}[\boldsymbol{\Xi}] \doteq & \exp\left[-\sum_{i=1}^{N} \mathrm{SNR}^{-\alpha_i + \beta_i}\right] \mathrm{SNR}^{-\sum_{i<j}^{N}(\alpha_i - \beta_j)^+} \\ & \cdot \mathrm{SNR}^{-\sum_{i=1}^{N+1}(L-N-1)\beta_i} \mathrm{SNR}^{-\sum_{i=N+2}^{L}(L-i)\beta_i} \\ & \cdot \mathrm{SNR}^{-\sum_{i=1}^{N}\sum_{N+1}^{L}(\alpha_i - \beta_j)^+}\end{aligned} \tag{66}$$

if $\alpha_i \geq \beta_i \forall 1 \leq i \leq N$, otherwise the determinant term decreases exponentially in SNR. Combining all the terms in (33) and $p(\boldsymbol{\beta})$ in (40) gives the form stated in the lemma.

REFERENCES

[1] D. Dobkin, *The RF in RFID*. Elsevier Inc., 2008.

[2] S. Roy, V. Jandhyala, J. Smith, D. Wetherall, B. Otis, R. Chakraborty, M. Buettner, D. Yeager, Y.-C. Ko, and A. Sample, "RFID: from supply chains to sensor nets," *Proc. IEEE*, vol. 98, no. 9, pp. 1583–1592, Sept. 2010.

[3] O. Akan, M. Isik, and B. Baykal, "Wireless passive sensor networks," *IEEE Commun. Mag.*, vol. 47, no. 8, pp. 92–99, 2009.

[4] "IEEE standard for local and metropolitan area networks—part 15.4: low-rate wireless personal area networks (LR-WPANs) amendment 2: active radio frequency identification (RFID) system physical layer (PHY)," IEEE Std 802.15.4f-2012 (Amendment to IEEE Std 802.15.4-2011), pp. 1–72, 2012.

[5] V. Chawla and D.-S. Ha, "An overview of passive RFID," *IEEE Commun. Mag.*, vol. 45, no. 9, pp. 11–17, 2007.

[6] S. Preradovic and N. Karmakar, "Chipless RFID: bar code of the future," *IEEE Microwave Mag.*, vol. 11, no. 7, pp. 87–97, 2010.

[7] F. Fuschini, C. Piersanti, F. Paolazzi, and G. Falciasecca, "Analytical approach to the backscattering from UHF RFID transponder," *IEEE Antennas and Wireless Propaga. Lett.*, vol. 7, pp. 33–35, 2008.

[8] A. Sample, D. Yeager, P. Powledge, and J. Smith, "Design of a passively-Powered, programmable sensing platform for UHF RFID systems," in *Proc. 2007 IEEE International Conference on RFID*, pp. 149–156.

[9] D. Yeager, P. Powledge, R. Prasad, D. Wetherall, and J. Smith, "Wirelessly-charged UHF tags for sensor data collection," in *Proc. 2008 IEEE International Conference on RFID*, pp. 320–327.

[10] EPC Global RFID Protocol Class 1 Generation 2 UHF, EPC Global, Jan. 2005.

[11] M. Buettner, B. Greenstein, A. Sample, J. R. Smith, and D. Wetherall, "Revisiting smart dust with RFID sensor networks," in *Proc2008 ACM Workshop on Hot Topics in Networks*.

[12] D. Yeager, J. Holleman, R. Prasad, J. Smith, and B. Otis, "Neuralwisp: a wirelessly powered neural interface with 1-m range," *IEEE Trans. Biomedical Circuits and Systems*, vol. 3, no. 6, pp. 379–387, 2009.

[13] D. Yeager, F. Zhang, A. Zarrasvand, and B. Otis, "A 9.2 microamp gen 2 compatible UHF RFID sensing tag with -12dbm sensitivity and 1.25 microvolt rms input-referred noise floor," in *Proc. 2010 IEEE International Solid-State Circuits Conference*, pp. 52–53.

[14] S. Thomas, R. Harrison, A. Leonardo, and M. Reynolds, "A battery-free multichannel digital neural/EMG telemetry system for flying insects," *IEEE Trans. Biomedical Circuits and Systems*, vol. 6, no. 5, pp. 424–436, 2012.

[15] L. Zhu and T. Yum, "Optimal framed Aloha based anti-collision algorithms for RFID systems," *IEEE Trans. Commun.*, vol. 58, no. 12, pp. 3583–3592, 2010.

[16] A. Bletsas, S. Siachalou, and J. Sahalos, "Anti-collision backscatter sensor networks," *IEEE Trans. Wireless Commun.*, vol. 8, no. 10, pp. 5018–5029, 2009.

[17] A. Bletsas, J. Kimionis, A. Dimitriou, and G. Karystinos, "Single-antenna coherent detection of collided fm0 RFID signals," *IEEE Trans. Commun.*, vol. 60, no. 3, pp. 756–766, 2012.

[18] C. Angerer, R. Langwieser, and M. Rupp, "RFID reader receivers for physical layer collision recovery," *IEEE Trans. Commun.*, vol. 58, no. 12, pp. 3526–3537, 2010.

[19] J. Wang, H. Hassanieh, D. Katabi, and P. Indyk, "Efficient and reliable low-power backscatter networks," in *Proc. 2012 ACM SIGCOMM Conference on Applications, Technologies, Architectures, and Protocols for Computer Communication*, ser. SIGCOMM '12, pp. 61–72. Available: http://doi.acm.org/10.1145/2342356.2342364

[20] M. Simon and D. Divsalar, "Some interesting observations for certain line codes with application to RFID," *IEEE Trans. Commun.*, vol. 54, no. 4, pp. 583–586, Apr. 2006.

[21] C. Boyer and S. Roy, "Hybrid ARQ improvements for RFID systems," in *Proc. 2013 IEEE International Conference on RFID*, pp. 223–230.

[22] G. D. Vita and G. Iannacone, "Design criteria for the RF section of UHF and microwave passive RFID transponders," *IEEE Trans. Microwave Theory and Techniques*, vol. 53, no. 9, pp. 2978–2990, Sept. 2005.

[23] T. Le, K. Mayaram, and T. Fiez, "Efficient far-field radio frequency energy harvesting for passively powered sensor networks," *IEEE J. Solid-State Circuits*, vol. 43, no. 5, pp. 1287–1302, 2008.

[24] C. Boyer and S. Roy, "Coded QAM backscatter modulation for RFID," *IEEE Trans. Commun.*, vol. 60, no. 7, pp. 1925–1934, 2012.

[25] F. Hessar and S. Roy, "Energy based performance evaluation of passive EPC GEN 2 class 1 RFID systems," *IEEE Trans. Commun.*, vol. 61, no. 4, pp. 1337–1348, 2013.

[26] R. Chakraborty, S. Roy, and V. Jandhyala, "Revisiting RFID link budgets for technology scaling: range maximization of RFID tags," *IEEE Trans. Microwave Theory and Techniques*, vol. 59, no. 2, pp. 496 –503, 2011.

[27] J. Griffin and G. Durgin, "Gains for RF tags using multiple antennas," *IEEE Trans. Antennas and Propag.*, vol. 56, no. 2, pp. 563–570, feb. 2008.

[28] S. Thomas and M. S. Reynolds, "QAM backscatter for passive UHF RFID tags," in *Proc. 2010 IEEE International Conference on RFID*, pp. 210–214.

[29] J. Griffin and G. Durgin, "Complete link budgets for backscatter-radio and rfid systems," *IEEE Antennas and Propag. Mag.*, vol. 51, no. 2, pp. 11–25, 2009.

[30] C. Boyer and S. Roy, "Space time coding for backscatter RFID," *IEEE Trans. Wireless Commun.*, vol. 12, no. 5, pp. 2272–2280, 2013.

[31] L. Zheng and D. Tse, "Diversity and multiplexing: a fundamental tradeoff in multiple-antenna channels," *IEEE Trans. Inf. Theory*, vol. 49, no. 5, pp. 1073–1096, 2003.

[32] U. Karthaus and M. Fischer, "Fully integrated passive UHF RFID transponder IC with 16.7- μ W minimum RF input power," *IEEE J. Solid-State Circuits*, vol. 38, no. 10, pp. 1602–1608, Oct. 2003.

[33] R. Hansen, "Relationships between antennas as scatterers and as radiators," *Proc. IEEE*, vol. 77, no. 5, pp. 659–662, 1989.

[34] J. Kimionis, A. Bletsas, and J. Sahalos, "Bistatic backscatter radio for tag read-range extension," in *Proc. 2012 International Conference on RFID-Technologies and Applications*, pp. 356–361.

[35] S. Thomas and M. Reynolds, "A 96 mbit/sec, 15.5 pj/bit 16-qam modulator for uhf backscatter communication," in *Proc. 2012 IEEE International Conference on RFID*, pp. 185–190.

[36] G. Vannucci, A. Bletsas, and D. Leigh, "A software-defined radio system for backscatter sensor networks," *IEEE Trans. Wireless Commun.*, vol. 7, no. 6, pp. 2170–2179, 2008.

[37] D. Dardari, R. D'Errico, C. Roblin, A. Sibille, and M. Win, "Ultrawide bandwidth RFID: the next generation?" *Proc. IEEE*, vol. 98, no. 9, pp. 1570–1582, 2010.

[38] U. Madhow, *Fundamentals of Digital Communication*. Cambridge, 2008.

[39] D. Costello and S. Lin, *Error Control Coding: Fundamentals and Applications*. Prentice-Hall, 1983.

[40] T. Cover and J. Thomas, *Elements of Information Theory*. John Wiley & Sons, 2006.

[41] J. Griffin and G. Durgin, "Multipath fading measurements at 5.8 GHz for backscatter tags with multiple antennas," *IEEE Trans. Antennas and Propag.*, vol. 58, no. 11, pp. 3693–3700, Nov. 2010.

[42] J. Griffin, "High-frequency modulated-backscatter communication using multiple antennas," Ph.D. dissertation, Georgia Institute of Technology, 2009.

[43] S. Loyka and A. Kouki, "On MIMO channel capacity, correlations, and keyholes: analysis of degenerate channels," *IEEE Trans. Commun.*, vol. 50, no. 12, pp. 1886–1888, Dec. 2002.

[44] D. Chizhik, G. Foschini, and R. Valenzuela, "Capacities of multi-element transmit and receive antennas: correlations and keyholes," *Electron. Lett.*, vol. 36, no. 13, pp. 1099–1100, Jun. 2000.

[45] P. Almers, F. Tufvesson, and A. Molisch, "Keyhole effect in MIMO wireless channels: measurements and theory," *IEEE Trans. Wireless Commun.*, vol. 5, no. 12, pp. 3596–3604, Dec. 2006.

[46] D. Tse and P. Viswanath, *Fundamentals of Wireless Communication*. Cambridge University Press, 2005.

[47] V. Tarokh, H. Jafarkhani, and A. Calderbank, "Space-time block codes from orthogonal designs," *IEEE Trans. Inf. Theory*, vol. 45, no. 5, pp. 1456–1467, Jul. 1999.

[48] E. Larsson and P. Stocia, *Space-Time Block Coding for Wireless Communications*. Cambridge University Press, 2008.

[49] S. Alamouti, "A simple transmit diversity technique for wireless communications," *IEEE J. Sel. Areas Commun.*, vol. 16, no. 8, pp. 1451–1458, Oct. 1998.

[50] V. Tarokh, N. Seshadri, and A. Calderbank, "Space-time codes for high data rate wireless communication: performance criterion and code construction," *IEEE Trans. Inf. Theory.*, vol. 44, no. 2, pp. 744–765, Mar. 1998.

[51] C. He, X. Chen, Z. J. Wang, and W. Su, "On the performance of MIMO RFID backscattering channels," *EURASIP J. Wireless Commun. and Networking*, vol. 2012, no. 1, p. 357, 2012. Available: http://jwcn.eurasipjournals.com/content/2012/1/357

[52] S. Yang and J. C. Belfiore, "Diversity-multiplexing tradeoff of double scattering MIMO channels," *IEEE Trans. Inf. Theory*, vol. 57, no. 4, pp. 2027–2034, 2011.

[53] E. Telatar, "Capacity of multi-antenna Gaussian channels," *European Trans. Telecommun.*, vol. 10, no. 6, pp. 585–595, 1999.

[54] N. Bleistein and R. Handlesman, *Asymptotic Expansion of Integrals*. Dover Publications, 1975.

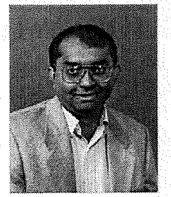
[55] A. Tulino and S. Verdu, *Random Matrix Theory and Wireless Communication*. Now Publishers, 2004.

[56] R. Narasimhan, "Finite-SNR diversity multiplexing tradeoff for correlated Rayleigh and Rician MIMO channels," *IEEE Trans. Inf. Theory*, vol. 52, no. 9, pp. 3965–3979, 2006.

[57] A. R. Koelle, S. W. Depp, and R. Freyman, "Short-range radio-telemetry for electronic identification, using modulated RF backscatter," *Proc. IEEE*, vol. 63, no. 8, pp. 1260–1261, 1975.



Colby Boyer Colby Boyer received the B.S. degree in Electrical Engineering and Computer Science from the University of California Berkeley in 2009. He joined Eta Kappa Nu in 2006 and IEEE as a student member in 2007. Currently he is pursuing a Ph.D. degree in Electrical Engineering at the University of Washington. His current research interests include low power wireless communication and its application to RFID. In the past, he has held summer internships at Los Alamos National Laboratory, Qualcomm Inc, and MIT Lincoln Labs.



Sumit Roy Sumit Roy received the B. Tech. degree from the Indian Institute of Technology (Kanpur) in 1983, and the M. S. and Ph. D. degrees from the University of California (Santa Barbara), all in Electrical Engineering in 1985 and 1988 respectively, as well as an M. A. in Statistics and Applied Probability in 1988. Presently, he is Prof. of Electrical Engineering, Univ. of Washington where his research interests include analysis/design of communication systems/networks, with an emphasis on next generation mobile/wireless and sensor networks. He spent 2001-03 on academic leave at Intel Wireless Technology Lab as a Senior Researcher engaged in research and standards development for ultra-wideband systems (Wireless PANs) and next generation high-speed wireless LANs. He served as Science Foundation of Ireland Isaac Walton Fellow during a sabbatical at University College, Dublin (Jan.-Jun. 2008) and was the recipient of a Royal Acad. Engineering (UK) Distinguished Visiting Fellowship during summer 2011. He was elevated to IEEE Fellow by the Communications Society in 2007 for his "contributions to multi-user communications theory and cross-layer design of wireless networking standards."